Journal of Nanobiotechnology

RESEARCH Open Access

Carbon dots derived from Ligusticum Chuanxiong mitigate cardiac injury by disrupting the harmful oxidative stress-apoptosis cycle

Yapeng Guo[1], Lei Yang[2], Li Yao[3], Chengdong Zhou[1], Yuanyuan Zhu[1], Chenxi Xu[1], Wenlong Wang[1], Jian Song[4], Mingzhen Zhang[1*] and Zhichao Deng[1*]

Abstract

Background Myocardial ischemia-reperfusion injury (MIRI) represents a significant complication following myocardial infarction surgery, for which preventive strategies remain limited. The primary pathological characteristics of MIRI include oxidative stress and apoptosis.

Results This study presents the synthesis of carbon dots derived from Ligusticum Chuanxiong (LC-CDs) through the application of the hydrothermal method. The LC-CDs show strong scavenging abilities for free radicals, effectively reducing oxidative stress and preventing apoptosis, which helps combat MIRI. The findings demonstrate that LC-CDs can effectively neutralize excessive ROS within cells, thereby alleviating oxidative stress, restoring mitochondrial function, and preventing DNA damage. Concurrently, LC-CDs suppress the polarization of M1-type macrophages and reduce the secretion of pro-inflammatory cytokines. Following the in situ administration of LC-CDs into the hearts of MIRI-model rats, a significant reduction in the necrotic area of the myocardium was observed, alongside the restoration of cardiac function, with no adverse reactions reported. Moreover, similar to the pharmacological effects of Ligusticum chuanxiong, LC-CDs can also inhibit apoptosis by protecting mitochondria and suppressing the expression of apoptotic proteins (Caspase3, Caspase9, and Bax).

Conclusions The intervention strategy employing LC-CDs, which targets oxidative stress and apoptosis in MIRI, holds promise as a potential model for the clinical treatment of MIRI.

Keywords Carbon dots, Ligusticum Chuanxiong, Myocardial ischemia-reperfusion injury, Oxidative stress, Apoptosis

*Correspondence:
Mingzhen Zhang
mzhang21@xjtu.edu.cn
Zhichao Deng
dzc3121115@stu.xjtu.edu.cn
[1]School of Basic Medical Sciences, Xi'an Jiaotong University, Xi'an, Shaanxi 710061, China
[2]Department of Cardiovascular Surgery, The First Affiliated Hospital of Xi'an Jiaotong University, Xi'an, Shaanxi 710061, China
[3]Department of Neurology, XD Group Hospital, Xi'an, Shaanxi 710077, China
[4]Institute of Cardiovascular Sciences, Guangxi Academy of Medical Sciences, The People's Hospital of Guangxi Zhuang Autonomous Region, Nanning, Guangxi 530021, China

Introduction

On a global scale, the incidence and mortality rates of myocardial infarction have been increasing year by year [1, 2]. Alarmingly, the frequency of myocardial infarction among people under 45 years old is rising steadily [3]. Clinically, reperfusion therapy achieved through percutaneous coronary intervention is the most effective approach for treating myocardial infarction [4]. However, for the heart, the ischemia-reperfusion process may exacerbate myocardial injury, which is known as myocardial ischemia-reperfusion injury (MIRI) [5]. During myocardial ischemia, due to the insufficient and untimely supply of oxygen and nutrients, myocardial cells mainly rely on anaerobic glycolysis to generate ATP [6]. In this process, a large amount of lactic acid accumulates, disrupting the normal function of the cell mitochondria. During the reperfusion phase, dysfunction of the respiratory chain fails to adapt to the returning oxygen supply, ultimately resulting in the excessive production of reactive oxygen species (ROS). At the same time, immune cells in the blood are activated during reperfusion. They penetrate the damaged walls of blood vessels, accumulate locally in the myocardium, and release numerous pro-inflammatory cytokines, which further exacerbate the damage to myocardial cells [7]. While reperfusion therapy is a critical intervention for mitigating myocardial infarction, there remains a deficiency in effective strategies for the prevention of myocardial ischemia-reperfusion injury (MIRI).

Traditional Chinese herbs have a long history of development and extensive clinical experience in treating heart diseases. A variety of traditional Chinese medicines, such as Ligusticum Chuanxiong, Astragalus membranaceus, Cinnamomum cassia twig, etc., have been applied in the treatment of MIRI [8–10]. Among them, the research related to Ligusticum Chuanxiong has drawn significant attention. Studies have shown that Ligusticum chuanxiong can alleviate the ischemia-reperfusion (I/R) injury of myocardial cells and inhibit the apoptosis of rat myocardial cells by down-regulating the expression levels of pro-apoptotic factors, including Caspase-3 [11]. Ligusticum Chuanxiong is included in numerous formulas and patent medicines for treating heart diseases [9]. Studies have indicated that multiple active components in Ligusticum Chuanxiong, such as tetramethylpyrazine and chuanxiong lactone, play crucial roles in alleviating MIRI [12, 13]. Tetramethylpyrazine can reduce oxidative stress during myocardial ischemia-reperfusion and mitigate apoptosis induced by reperfusion by activating the antioxidant function of HO-1 [14]. Simultaneously, it can also exert a cardioprotective function by regulating the PI3K/Akt/GSK-3β pathway [15]. Chuanxiong lactone plays an important role in enhancing thrombin activity, promoting vascular repair, and providing antithrombotic effects [16]. In the oxygen-glucose deprivation/reoxygenation (OGD/R) model, chuanxiong lactone can attenuate the nuclear translocation of the NF-κB pathway in cells and inhibit the TLR4/NF-κB pathway, thus relieving ischemia-reperfusion injury [17]. Nevertheless, the clinical application of Ligusticum Chuanxiong is limited by its poor water solubility and the challenges associated with extracting its active constituents. Furthermore, akin to other traditional Chinese medicinal herbs, Ligusticum Chuanxiong exhibits low oral bioavailability and significant inter-individual variability in absorption and metabolism. These factors impede the attainment of consistent therapeutic outcomes in clinical settings and complicate the optimization of pharmacological regimens.

As a novel nanomaterial, carbon dots (CDs) derived from traditional Chinese herbs have been extensively studied in recent years [18–21]. They integrate the advantages of traditional Chinese herbs and modern nanotechnology, demonstrating great potential in the field of disease treatment research. Research indicates that CDs possess a relatively large π-π conjugated sp^2 plane, which endows them with excellent electrical conductivity and a unique geometric structure [22]. In the catalytic field, CDs have proven to exhibit good catalytic efficiency, demonstrating peroxidase-like (POD) [23, 24], catalase-like (CAT) [25], and superoxide dismutase-like (SOD) activities [26, 27]. Consequently, they have found applications in the research of various diseases. Gao et al. discovered that the catalytic activity of CDs stems from the oxygen-containing functional groups on their surface and the large sp^2 plane [27]. The abundant oxygen-containing functional groups on the surface of CDs also confer good water solubility to them [28]. Moreover, the surface states of CDs not only endow them with catalytic activity, but the surface polymers formed through polymerization, cross-linking, and carbonization also endow CDs with the molecular properties of the precursor materials [29]. Currently, extensive applied research on CDs derived from traditional Chinese herbs has been carried out in areas such as anti-inflammation [30], anti-tumor [31], and hemostasis [20].

In this study, we successfully synthesized LC-CDs using Ligusticum Chuanxiong as a carbon source precursor through the hydrothermal method. This approach significantly addressed the low bioavailability of Ligusticum Chuanxiong and the difficulties associated with its clinical application. LC-CDs exhibited strong ROS-scavenging capabilities, effectively reducing oxidative stress. They improved mitochondrial dysfunction caused by ischemia-reperfusion and inhibited the polarization of M1-type macrophages, thereby diminishing the inflammatory response and countering MIRI. In the rat model of MIRI, when LC-CDs were administered via local myocardial injection, they demonstrated remarkable

cardioprotective effects and exhibited excellent safety profiles. We used transcriptomics to explore the potential mechanisms through which LC-CDs treat MIRI. The results of this study demonstrate that LC-CD can significantly improve the pathological microenvironment caused by MIRI by alleviating the oxidative stress response. Mechanistic studies indicate that LC-CD inherits the core pharmacological activities of Ligusticum chuanxiong. It can effectively inhibit the process of myocardial cell apoptosis by suppressing the expression of key proteins related to apoptosis, such as Bax, Caspase-9, and Caspase-3, thereby reducing the degree of MIRI damage (Fig. 1). LC-CDs, synthesized from Ligusticum chuanxiong, feature a more precisely defined structure and catalytic mechanism. The uncomplicated one-step hydrothermal synthesis method not only simplifies the manufacturing process but also facilitates the scalable production of LC-CDs, making them suitable for industrial applications. Compared with other nanomaterials, LC-CDs derive from biogenic sources, endowing them with enhanced biosecurity. These unique characteristics collectively endow LC-CDs with significant potential for treating MIRI, positioning them as a promising candidate for further translational research and clinical development in this challenging medical field.

Materials and methods

Materials

Ligusticum Chuanxiong was purchased from China National Traditional Chinese Medicine Co., Ltd. Nitrotetrazolium blue chloride (NBT), riboflavin, L-Methionine, 3,3',5,5'- Tetramethylbenzidine (TMB), FeSO4 (AR),

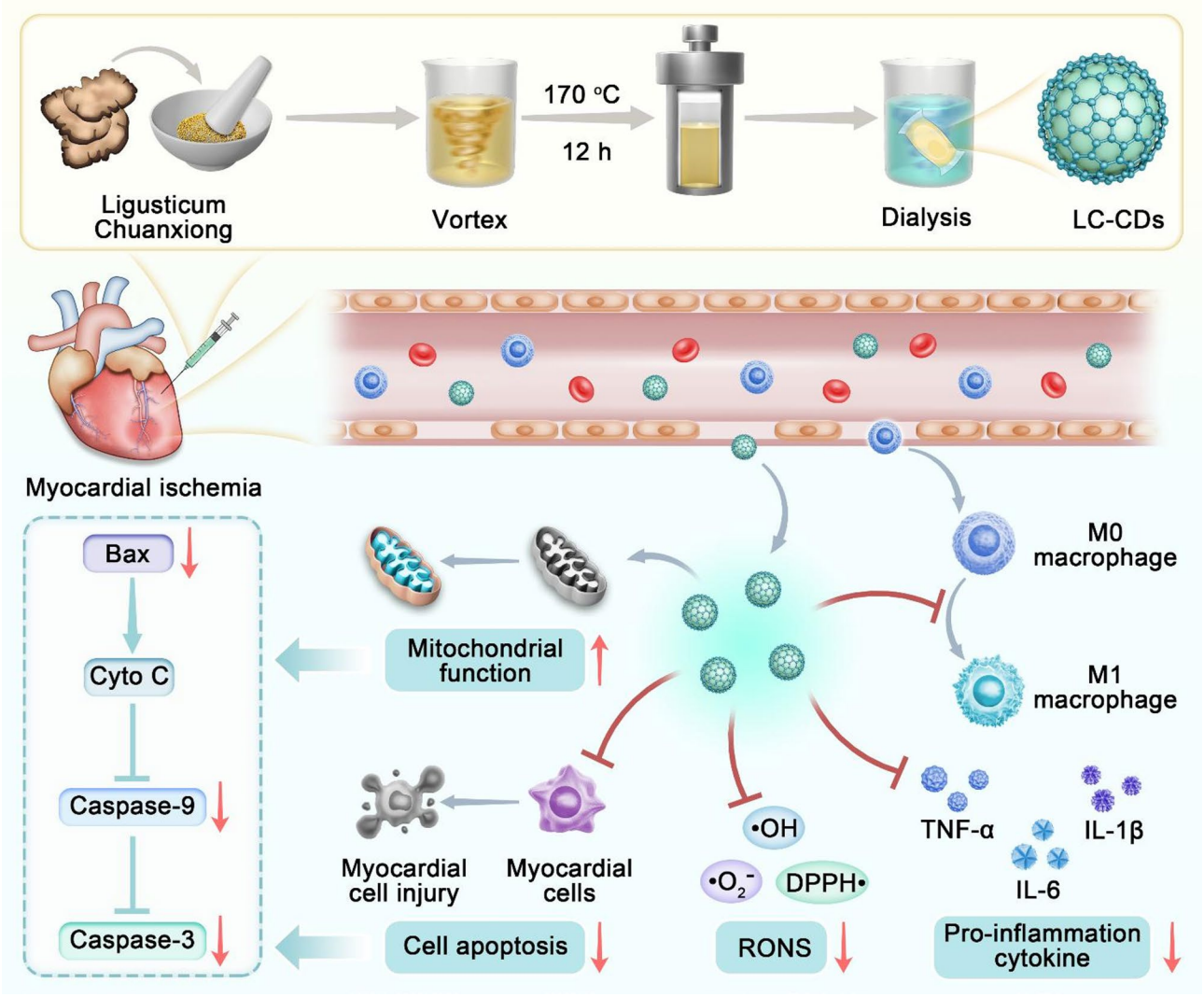

Fig. 1 Preparation of Ligusticum Chuanxiong-derived CDs and the mechanism of alleviating MIRI. LC-CDs were prepared *via* a one-step hydrothermal method. LC-CDs possess the ability to scavenge multiple types of free radicals. LC-CDs alleviate MIRI ultimately by alleviating oxidative stress, inhibiting cellular inflammation, and restoring mitochondrial function. LC-CDs play a significant role in alleviating apoptosis in MIRI

$K_2S_2O_8$, and 1,1–Diphenyl–2–picrylhydrazyl (DPPH) were purchased from McLean. H_2O_2 (30% in water) was obtained from Beijing Chemical Works. PBS (1×, pH 7.2–7.4) Purchased from Adamas-beta®. The specific medium for Raw264.7 cells was purchased from New Cell & Molecular Biotech Co. Cy5.5-amino was purchased from Xi'an Ruixi Biotechnology Co., Ltd. Goat Anti-Rat IgG/SAlexa Fluor 488 was purchased from Beijing Solarbio Science & Technology Co. Caspase-3 Rabbit pAb (A11319), Caspase-9 Rabbit mAb (A18676), Bax Rabbit mAb (A19684), 2X Universal SYBR Green Fast qPCR Mix (RK21203) and ABScript II Reverse Transcriptase (RK21400) were purchased from ABclonal.

Drug screening and network pharmacology process

The retrieval operation is performed in the prescription database of Huabing Data (http://www.huabeing.com) using "Myocardial Ischemia-Reperfusion" as the keyword. Through this search, relevant traditional Chinese medicine prescriptions are retrieved, and the drugs contained in these prescriptions are systematically sorted out, thereby screening out the drugs with the highest usage frequencies.

The comprehensive excavation of all the active ingredients of Ligusticum Chuanxiong is carried out by utilizing the Traditional Chinese Medicine Systems Pharmacology Database and Analysis Platform (TCMSP, http://lsp.nwsuaf.edu.cn/tcmsp.php). Given the large number of active ingredients, screening criteria are set based on pharmacokinetic parameters. Specifically, an oral bioavailability (OB) of not less than 30% and a drug-likeness (DL) of not less than 0.18 are used as the standards for screening active ingredients. The active ingredients that meet these criteria will be the objects of subsequent research. Additionally, the active ingredients used for the quality control of Ligusticum Chuanxiong medicinal materials in the Chinese Pharmacopoeia are also encompassed.

With the aid of the gene card retrieval tool, the gene targets related to "Myocardial Ischemia-Reperfusion" are searched by entering the keyword. Meanwhile, using the same keyword "Myocardial Ischemia-Reperfusion", relevant targets of myocardial ischemia-reperfusion are searched. Subsequently, the intersection of the active ingredient targets of Ligusticum Chuanxiong and the disease targets is obtained and presented in the form of a Venn diagram.

The potential targets of Ligusticum Chuanxiong for treating myocardial ischemia-reperfusion are input into the STRING database platform (https://string-db.org), with the species restricted to "Homo sapiens", and the corresponding predicted targets are obtained and stored as a TXT file. Subsequently, by using Cytoscape 3.9.1 software, the PPI graph is optimized in terms of networking and visualization according to established conditions. By clicking on the Network Analyzer plugin in the software, network analysis is conducted, including the analysis of topological values such as betweenness centrality, degree centrality, and closeness centrality. On this basis, the top 40 targets ranked by degree value are selected for in-depth analysis.

The Metascape database is applied to conduct GO (Gene Ontology) analysis operations on the 40 key targets at the intersection of Ligusticum Chuanxiong and myocardial ischemia-reperfusion that have been screened out.

Synthesis of LC-CDs by hydrothermal method

LC-CDs are synthesized through a simple one-step hydrothermal process. The specific procedure involves dispersing 200 mg of ground Ligusticum Chuanxiong powder in 20 mL of deionized water. After 1 h, the resulting solution is moved to a high-pressure sealed reactor and heated at 170 °C for 12 h [32]. The post-reaction solution appears black-brown. The solution is passed through a 0.22 μm filter and dialyzed using a 1000 Da dialysis bag for three days, yielding LC-CDs with uniform particle size.

Antioxidant capacity testing of LC-CDs

Superoxide Radical Scavenging Test: Prepare a 0.05 M phosphate buffer solution, a 130 mM methionine solution, a 750 μM nitroblue tetrazolium solution, a 100 μM EDTA-Na_2 solution, and a 20 μM riboflavin solution. These solutions are mixed in equal proportions, and solutions of LC-CDs at different concentration gradients are added. Under the close irradiation of an LED lamp, the solution changes color under the combined action of superoxide anions and LC-CDs. The scavenging rate of superoxide anions is detected and calculated using a microplate reader at 560 nm. Hydroxyl Radical Scavenging Test: A Fenton reaction system is constructed using 10 μM ferrous ions and 50 μM H_2O_2 to generate hydroxyl radicals. 0.3 mM TMB is used as a chromogenic agent to detect the content of hydroxyl radicals in this system. LC-CDs at different concentration gradients are prepared to react with the Fenton system. After the reaction, the scavenging efficiency of hydroxyl radicals is detected and calculated using a microplate reader at 652 nm. Electron paramagnetic resonance (EPR) spectra were measured on a CIQTEK EPR200M with continuous-wave X-band frequency.

Sub-organelle co-localization of LC-CDs with cells

Raw264.7 cells were co-incubated with LC-CDs at a concentration of 5 μg/mL for 3 h. Upon completion of the incubation, Lyso-tracker and Mito-tracker were employed to specifically stain lysosomes and mitochondria within the cells, respectively. Subsequently, cell slides

were prepared, and the co-localization of LC-CDs with mitochondria and lysosomes was meticulously observed using a laser confocal microscope.

Antioxidant capacity evaluation of LC-CDs at the cellular level

Oxidative stress injury systems were constructed using Raw264.7 and H9C2 cells as cell models. H_2O_2 was selected as the inducer. For Raw264.7 cells, the induction concentration was determined to be 600 μM, while for H9C2 cells, the induction concentration was set at 150 μM. LC-CDs at concentrations of 5 μg/mL and 10 μg/mL were separately incubated with the two types of cells mentioned above. After the incubation, DCFH and DHE fluorescent dyes were utilized to detect the oxidative stress levels of the cells. The treated cells were collected for laser confocal fluorescence imaging and flow cytometry experiments to quantitatively analyze the changes in the intracellular redox state.

Anti-inflammatory capacity evaluation of LC-CDs at the cellular level

LPS at a concentration of 500 ng/mL was adopted as the inducer to trigger the inflammatory response in Raw264.7 cells. LC-CDs at concentrations of 5 μg/mL and 10 μg/mL were co-incubated with the cells for 6 h to inhibit the inflammatory process. The real-time fluorescence qPCR technique was applied to evaluate the mRNA expression levels of pro-inflammatory cytokines (such as TNF-α, IL-1β, and IL-6) to measure the anti-inflammatory effect of LC-CDs.

Myocardial ischemia-reperfusion model

After anesthetization, the rats were secured supine on the operating table. The skin was incised between the 3rd and 4th intercostal spaces along the left sternal border. Blunt dissection of the intercostal muscles was performed to open the thoracic cavity, fully exposing the heart. A 7 – 0 silk thread was used to ligate the left anterior descending branch of the coronary artery. After ligation for 45 min, the slipknot of the ligature was loosened to restore the blood flow in the coronary artery. Thus, the rat model of MIRI was successfully constructed and could be used for subsequent related research.

Biosafety assessment in vitro

In vitro Biosafety Assessment at the Cellular Level. In vitro, biosafety assessments were conducted using Raw264.7 and H9C2 cell lines. LC-CDs solutions with concentration gradients of 0 μg/mL, 5 μg/mL, 10 μg/mL, 20 μg/mL, 30 μg/mL, 40 μg/mL, 50 μg/mL, 100 μg/mL, and 200 μg/mL were prepared and separately incubated with these two types of cells for 12 h and 24 h. Subsequently, a cell culture medium containing 20 μg/mL MTT was added to the cells, and the incubation was continued for another 4 h. Following incubation, the formazan product was dissolved in dimethyl sulfoxide (DMSO). Absorbance values from each well were quantified using a microplate reader to determine cell viability, thus assessing the effect of LC-CDs on cellular health.

Biosafety assessment in vivo

The in vivo biosafety experiment was conducted on a rat model. LC-CDs were administered to rats via local myocardial injection. After three consecutive days of observation, the major organs of the rats, including the heart, liver, spleen, lung, and kidney, as well as blood samples, were collected. The major organs were subjected to H&E staining for pathological section preparation. Tissue morphology was examined microscopically to evaluate potential damage. Meanwhile, blood biochemical index analysis and blood routine tests were performed on the blood samples to evaluate the impact of LC-CDs on the overall physiological functions of the rats.

Statistical analysis

Statistical analyses were performed using GraphPad Prism 7 software. Statistical comparisons were made using one-way ANOVA and a t-test. Statistical comparisons were made. Statistical significance was indicated as $^{*}p < 0.05$, $^{**}p < 0.01$, $^{***}p < 0.001$. $^{****}p < 0.0001$.

Results and discussion

The relationship between ligusticum chuanxiong and MIRI

MIRI is one of the most severe complications following surgical operations for myocardial infarction in clinical practice [33]. An in-depth analysis of the relationship between MIRI and oxidative stress, as well as its specific pathogenesis, is crucial for enhancing clinical treatment and improving patient prognosis. To thoroughly explore the pathogenesis of MIRI, this study obtained high-throughput sequencing expression profile data from the Gene Expression Omnibus (GEO) and conducted research using the Gene Set Enrichment Analysis (GSEA) method. The gene expression datasets of the hearts from the control group and MIRI-modeled rats (GEO acc + ession number: GSE240847) were utilized in this study. GSEA results showed that DEGs were significantly enriched in apoptosis-related signaling pathways within the Gene Ontology (GO) gene set (Fig. 2A). Meanwhile, the research findings also demonstrated that the pathogenesis of MIRI is closely linked to multiple redox-related pathways (Fig. 2B, C, and Fig. S1). This study further examined several genes associated with apoptosis, specifically Caspase9, Caspase3, Bax, and PAK1, by analyzing their expression levels. The results indicated that these genes were upregulated in the MIRI rat model, confirming the activation of the apoptosis pathway. This finding

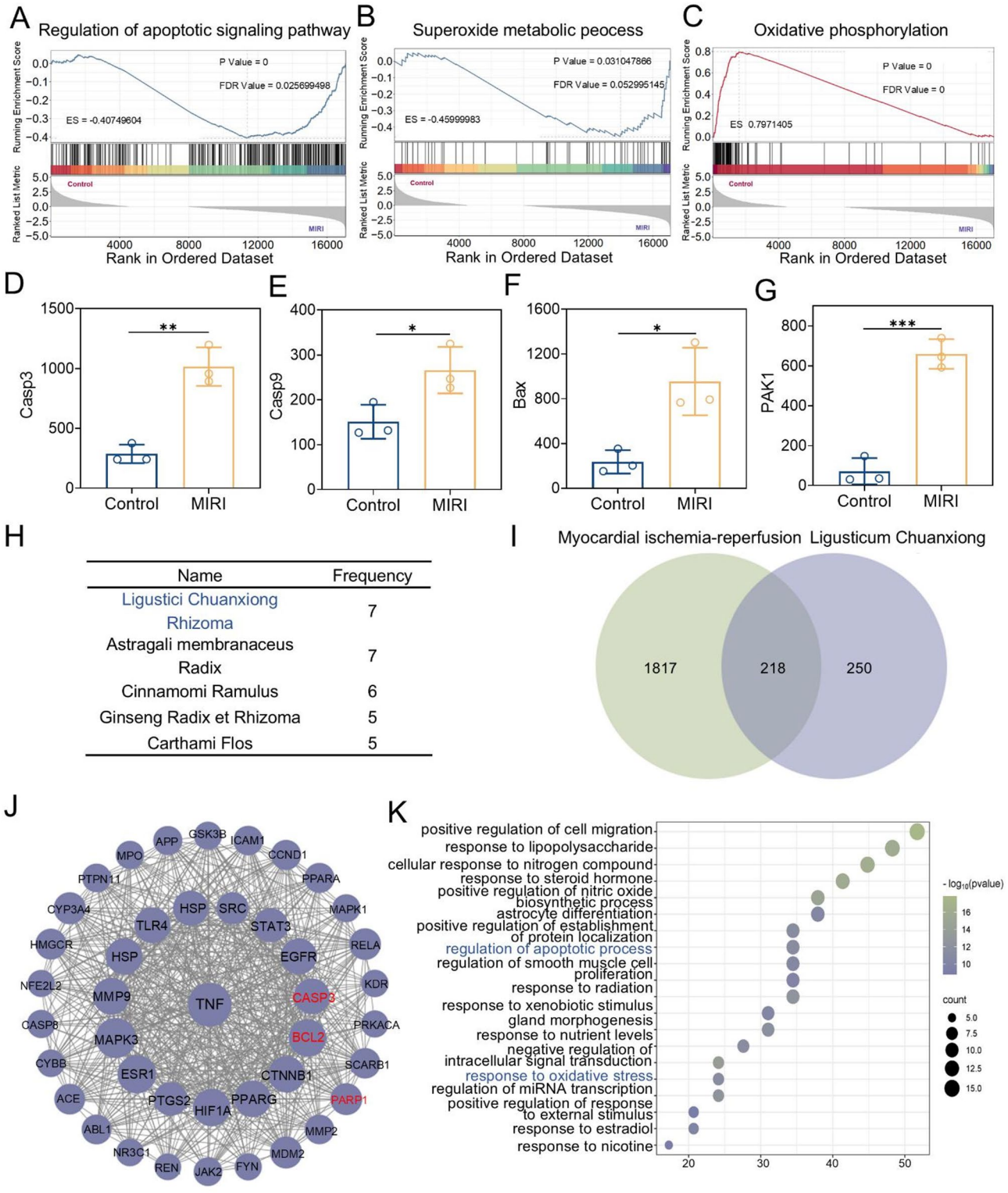

Fig. 2 The relationship between Ligusticum Chuanxiong and MIRI. (**A**-**C**) GSEA of differentially expressed genes between the Control group and MIRI rats (GEO accession no. 240847). (**D**-**G**) Comparison of the gene expression levels of the apoptosis signaling pathway among different groups (Casp3, Casp9, Bax, and PAK1). (**H**) The top five drugs in terms of frequency. (**I**) Venn diagram of the intersection of the targets of the active ingredients of Ligusticum Chuanxiong and disease-related targets. (**J**) Protein-protein interaction network of 40 key targets. (**K**) GO pathway enrichment analysis. Statistical comparisons were made using one-way ANOVA and t-test. Statistical significance was indicated as $*p < 0.05$, $**p < 0.01$, $***p < 0.001$. Data are expressed as mean ± SD ($n = 3$)

establishes a strong correlation between MIRI and apoptosis (Fig. 2D-G).

Ligusticum Chuanxiong has a long history of use in treating heart diseases.[8] In current clinical practice, it is often used as an adjuvant drug for the treatment of MIRI. However, the intrinsic relationship between Ligusticum Chuanxiong and MIRI remains unclear. This research explored the link between Ligusticum Chuanxiong and MIRI through drug screening and network pharmacology. Firstly, through drug screening, Ligusticum Chuanxiong was identified as a key traditional Chinese medicine for the treatment of MIRI. Using "myocardial ischemia-reperfusion" as the keyword, relevant Traditional Chinese medicine prescriptions were retrieved from the prescription database of Huabing Data (http://www.huabeing.com), and the drugs in the prescriptions were sorted and analyzed. The results showed that Ligusticum Chuanxiong and Astragali membranaceus were the drugs with the highest frequency of use (Fig. 2H). Subsequently, all the active ingredients of Ligusticum Chuanxiong were mined using the Traditional Chinese Medicine Systems Pharmacology Database and Analysis Platform (TCMSP, https://tcmsp-e.com/tcmsp.php). Given the numerous active ingredients of Ligusticum Chuanxiong, screening conditions were set based on pharmacokinetic parameters. Oral bioavailability (OB) ≥ 30% and drug-likeness (DL) ≥ 0.18 were set as the screening criteria. Finally, 10 active ingredients were selected as the research objects (Table S1). These 10 active ingredients were uploaded to the Swiss Target Prediction platform for target analysis, yielding 672 potential targets. At the same time, 2036 targets related to myocardial ischemia-reperfusion were obtained from the Gene Cards database. The overlap between Ligusticum Chuanxiong's predicted targets and myocardial ischemia-reperfusion targets was analyzed, resulting in 218 shared targets (Fig. 2I). These 218 mapped targets were uploaded to the STRING database to generate the TSV file of the PPI network, subsequently analyzed using Cytoscape 3.10.1. In Cytoscape, targets with high dispersion were removed, and the "Network Analyzer" function was used to evaluate the topological characteristics of the results. The top 40 targets with the highest degree values were selected as key targets. Visualization was performed on the 40 key targets obtained by screening to construct and analyze the protein-protein interaction network (Fig. 2J). Finally, the 40 key targets were uploaded to the Metascape database for Gene Ontology (GO) pathway enrichment analysis. The findings revealed that Ligusticum Chuanxiong's connection to MIRI is strongly linked to oxidative stress and apoptosis signaling pathways (Fig. 2K). In conclusion, we believe that Ligusticum Chuanxiong is a promising drug for reducing MIRI by targeting oxidative stress and apoptosis pathways.

Synthesis and characterization of LC-CDs

The difficulties in isolating the active constituents of Ligusticum Chuanxiong, coupled with its limited oral bioavailability and additional constraints, have impeded its application in clinical practice. To effectively address this issue, LC-CDs were successfully synthesized using a simple one-step hydrothermal method. The fresh Chinese herbal medicine Ligusticum chuanxiong was dried and ground into powder. Subsequently, LC-CDs were successfully obtained through a simple one-step hydrothermal synthesis method. During multiple synthesis processes, the yields of LC-CDs were relatively similar, approximately 10%. The transmission electron microscopy (TEM) image of LC-CDs is presented in Fig. 3A. The image demonstrates that LC-CDs possess excellent dispersibility and exhibit a morphology that is approximately quasi-spherical. The inset in Fig. 3A is the statistical result of the particle sizes of LC-CDs. This suggests that LC-CDs exhibit a narrow size distribution, with an average diameter of around 2.4 ± 0.03 nm (Fig. 3A). The extremely small particle size of LC-CDs indicates that it has a high specific surface area, which enables LC-CDs to expose more active sites and thus fully exert their functions. To further investigate the microscopic structural characteristics of LC-CDs, a high-resolution transmission electron microscope (HRTEM) was used to meticulously examine their lattice. After precise measurement, the lattice spacing of LC-CDs was found to be 0.21 nm, which corresponds to the (100) crystal plane of graphite, strongly demonstrating that LC-CDs possess a graphite-like phase structure (Fig. 3B). When CDs possess graphitized lattices with a spacing of 0.21 nm, their atomic arrangement exhibits a highly ordered π-π conjugate system. This structural feature provides an ideal condition for the formation of delocalized large π bonds. In the catalytic process, the presence of delocalized large π bonds significantly enhances the delocalization degree of the electron cloud, not only reducing the electron transfer resistance of the system but also effectively promoting the directional migration of electrons between the active sites and reactants, thus remarkably improving the electron transfer efficiency and overall performance of the catalytic reaction. The fluorescence property is one of the key properties of CDs. This research thoroughly investigated the fluorescence behavior of LC-CDs under varying excitation wavelengths. As shown in Fig. 3C under multiple excitation wavelengths, the optimal emission wavelengths of LC-CDs were predominantly concentrated around 450 nm. Further, by detecting the fluorescence decay curve of LC-CDs and through precise calculation, its fluorescence lifetime was obtained as 3.56 ns (Fig. 3D). In a dark environment, when LC-CDs were irradiated with ultraviolet light, it could be observed that they emitted blue-green fluorescence (Fig. S2). The

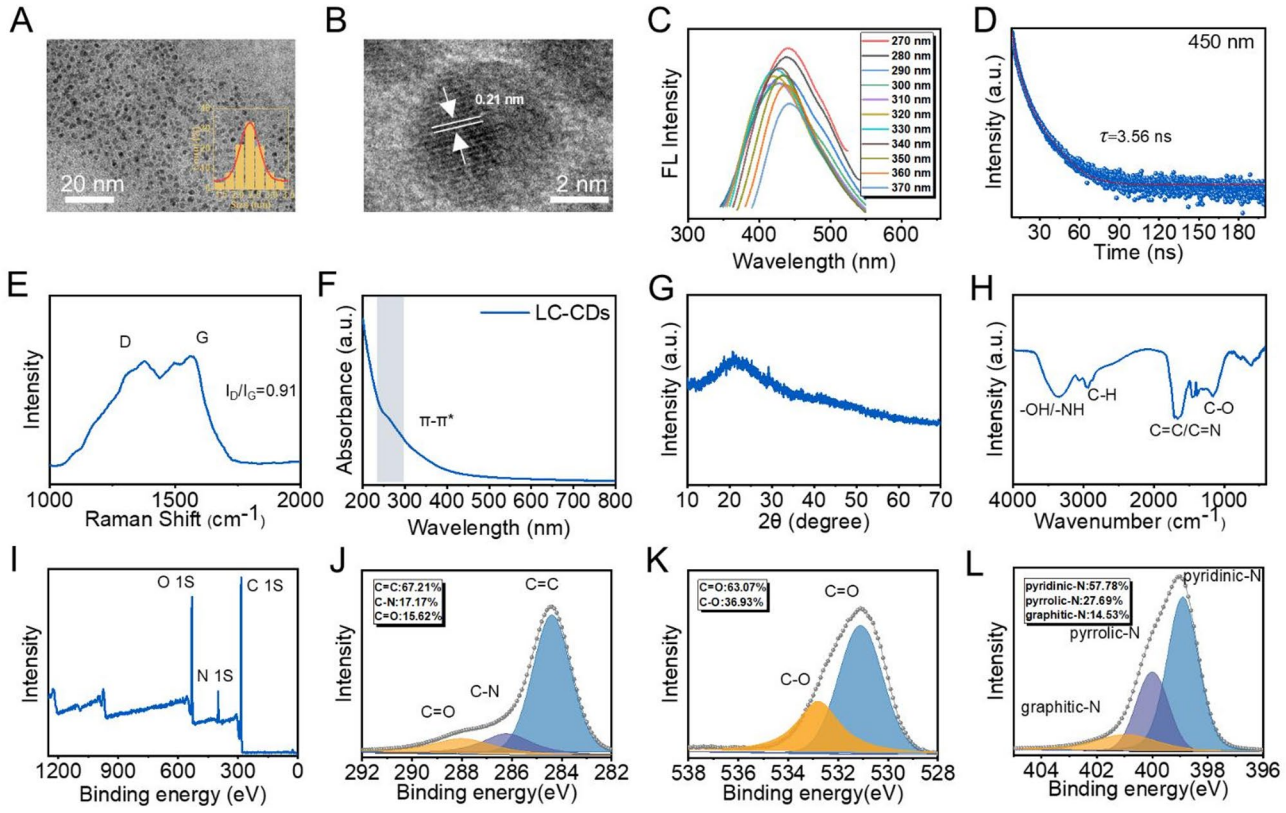

Fig. 3 Synthesis and characterization of LC-CDs. (**A**) TEM and size distribution histogram of LC-CDs. (**B**) HR-TEM of Ca-CDs. (**C**) Emission spectra of LC-CDs under different excitations. (**D**) Fluorescence lifetime of LC-CDs. (**E**) Raman spectrum and (**F**) UV-vis spectrum of LC-CDs. (**G**) XRD spectrum and (**H**) FT-IR spectrum of LC-CDs. (**I**) XPS survey spectra of LC-CDs. (**J**-**L**) High-resolution XPS spectra of C 1s, O 1s, and N 1s for LC-CDs

above-mentioned phenomena fully indicate that the CDs derived from Ligusticum Chuanxiong have been successfully synthesized. Raman spectroscopy was used to accurately measure the degree of graphitization and surface defects in LC-CDs. In the Raman spectrum, the D peak around 1300 cm^{-1} reflects the defect state of the carbon lattice, while the G peak near 1580 cm^{-1} corresponds to the sp^2 hybridized carbon's in-plane vibrational mode, indicating the graphitization level of LC-CDs. Raman spectroscopy revealed the coexistence of D and G peaks in the LC-CDs spectrum, with an ID/IG ratio of 0.91 (Fig. 3E). This result indicates that LC-CDs not only have a relatively high graphitization degree but also have a large number of defect sites on their surface. These surface defects and the π-π planar structure conducive to rapid electron transfer are highly likely to endow LC-CDs with remarkable catalytic properties. The ultraviolet absorption spectroscopy analysis results showed that LC-CDs exhibited a relatively broad absorption band in the wavelength range of 200–600 nm (Fig. 3F). This phenomenon is mainly attributed to the π-π* transition and n-π* transition existing in the carbon-dot structure. Among them, the π-π* transition originates from the presence of the sp^2-hybridized structure in the carbon core. Under ultraviolet light irradiation, π-bonded electrons are excited from the π orbital to the π* orbital [34]. The n-π transition arises from surface functional groups like -NH_2, -OH, and -COOH, enabling non-bonding electrons to transition to the π orbital upon photon absorption. These functional groups also provide a material basis for LC-CDs to exert their functions. The X-ray diffraction (XRD) experiment further characterized the crystal structure of LC-CDs. The XRD pattern showed that LC-CDs have a relatively broad diffraction peak at 21.4°, which could be attributed to the (002) plane of graphite. Through calculation, the d-spacing corresponding to this diffraction peak was approximately 0.42 nm (Fig. 3G). Subsequently, Fourier-transform infrared spectroscopy (FT-IR) and X-ray photoelectron spectroscopy (XPS) were used to further and meticulously characterize the surface structure of LC-CDs. In the FT-IR spectrum, the broad absorption peak at 3375 cm^{-1} could be attributed to the stretching vibration of-OH/-NH; the absorption peak at 2950 cm^{-1} originated from the symmetric and asymmetric stretching vibrations of methyl and methylene groups (C-H) in saturated hydrocarbons; the absorption peak at 1661 cm^{-1} corresponded to the absorption peak of the C = C double bond in the conjugated system or the stretching vibration of the C = N bond; the absorption peak at 1180 cm^{-1} was caused by

the stretching vibration of the C-O bond (Fig. 3H). These peaks confirm that LC-CDs possess abundant surface functional groups. The XPS analysis showed that LC-CDs are mainly composed of three elements: C, N, and O. Among them, the C1s peak had the highest intensity, with a corresponding content of 73.01%; the contents of O1s and N1s are 19.87% and 7.12%, respectively (Fig. 3I). Further, the XPS spectrum was subjected to peak-fitting processing for different elements. In the C1s spectrum, the peak at 248.4 eV corresponded to the C = C bond, the peak at 286.3 eV corresponded to the C-N bond, and the peak at 287.9 eV corresponded to the C = O; in the O1s spectrum, the peak at 531.1 eV corresponded to the C = O, and the peak at 532.8 eV corresponded to the C-O; in the N1s spectrum, the peaks at 398.9 eV, 400.07 eV, and 400.93 eV represented pyridinic-N, pyrrolic-N, and graphitic-N respectively. The detailed analysis results showed that in the C1s spectrum, the content of C = C was the highest, reaching 67.21%, and the contents of C-N and C = O were 17.17% and 15.62% respectively; in the O1s spectrum, the contents of C = O and C-O were 63.07% and 36.93% respectively; in the N1s spectrum, the contents of pyridinic-N, pyrrolic-N, and graphitic-N were 57.78%, 27.69%, and 14.53% respectively (Fig. 3J-L). The characterization results of XPS conclusively confirm that the chemical groups contained in Ligusticum chuanxiong are retained on the surface of LC-CDs. These groups constitute the material basis for LC-CDs to exert their pharmacological activities, providing crucial structural support for the realization of their biological functions. In conclusion, our thorough and systematic structural characterization of LC-CDs has confirmed their successful synthesis. The abundance of surface functional groups on LC-CDs enables potential pharmacological and catalytic functionalities. This finding greatly motivates us to further explore the potential applications of LC-CDs in relevant fields.

Free radical scavenging evaluation of LC-CDs

Within the carbon core structure, carbon atoms are arranged in a closely packed manner [35]. This highly ordered arrangement pattern can significantly reduce the energy gap width between carbon atoms [36]. According to the band theory, the reduction of the energy gap width implies a decrease in the energy required for electron transition [36]. Valence band electrons can be readily promoted through the absorption of modest energy inputs to traverse the forbidden energy gap and populate the conduction band. This electronic transition mechanism facilitates a marked increase in charge carrier density, as the delocalized electrons in the conduction band exhibit substantially enhanced mobility. The resultant elevation in free carrier population directly correlates with improved charge transport characteristics, thereby significantly enhancing the carbon-core material's conductivity performance. The excellent electron-transfer properties of CDs can endow them with good catalytic activity. The research by Gao et al. has demonstrated that CDs derived from activated carbon possess ultra-high SOD activity [26]. Through surface-group capping experiments and numerous studies, it has been shown that the SOD activity of CDs stems from the combination of hydroxyl and carboxyl groups with superoxide anions, as well as the electron transfer carried out by carbonyl groups conjugated with the π-system. In our previous research, we also verified that CDs derived from Honeysuckle (Hy-CDs) exhibit strong SOD activity. In that research, we verified that the SOD activity of Hy-CDs is chiefly derived from a substantial quantity of amino groups on their surface. Building on this foundation, we systematically investigated the catalytic properties of LC-CDs. First, we examined the ability of LC-CDs to scavenge $\cdot O_2^-$. A generation system of $\cdot O_2^-$ was constructed using riboflavin and methionine. Upon light exposure, riboflavin absorbs photon energy, undergoes excitation, and donates electrons to methionine, self-oxidizing to generate a semiquinone radical. The semiquinone radical reacts with molecular oxygen to generate $\cdot O_2^-$. The $\cdot O_2^-$ generated in the system oxidizes nitroblue tetrazolium chloride (NBT) to blue-violet NBT formazan, which has a strong absorption at 560 nm (Fig. 4A). This system can be used to detect the scavenging effect of LC-CDs on $\cdot O_2^-$. We first tested the kinetics of LC-CDs in scavenging $\cdot O_2^-$ using this system. The UV absorption of solutions containing different concentrations of LC-CDs at 560 nm was continuously monitored within 520s. The results showed that as time elapsed, the absorption of the system solution without LC-CDs at 560 nm gradually increased, indicating that a large amount of $\cdot O_2^-$ was generated in the solution. However, after adding LC-CDs, the UV absorption of the solution decreased significantly, suggesting that LC-CDs can remarkably inhibit the generation of $\cdot O_2^-$ (Fig. 4B). Especially as the concentration of LC-CDs attained 60 μg/mL, the absorption of the solution at 560 nm hardly changed. Subsequent UV-Vis spectral analysis (500–800 nm) of the post-reaction solution revealed absorption characteristics that closely mirrored the time-dependent kinetic behavior observed in the chemical reaction (Fig. 4C). The final statistical results showed that as the concentration of LC-CDs increased, their ability to scavenge $\cdot O_2^-$ gradually enhanced. As the concentration of LC-CDs attained 60 μg/mL, the scavenging rate of $\cdot O_2^-$ nearly reached 100% (Fig. 4D). These results indicate that LC-CDs possess strong SOD-like enzyme activity. Immediately after, we examined the ability of LC-CDs to scavenge hydroxyl radicals (·OH). ·OH is a key element causing and aggravating the physiological imbalance in the human body. We simulated the

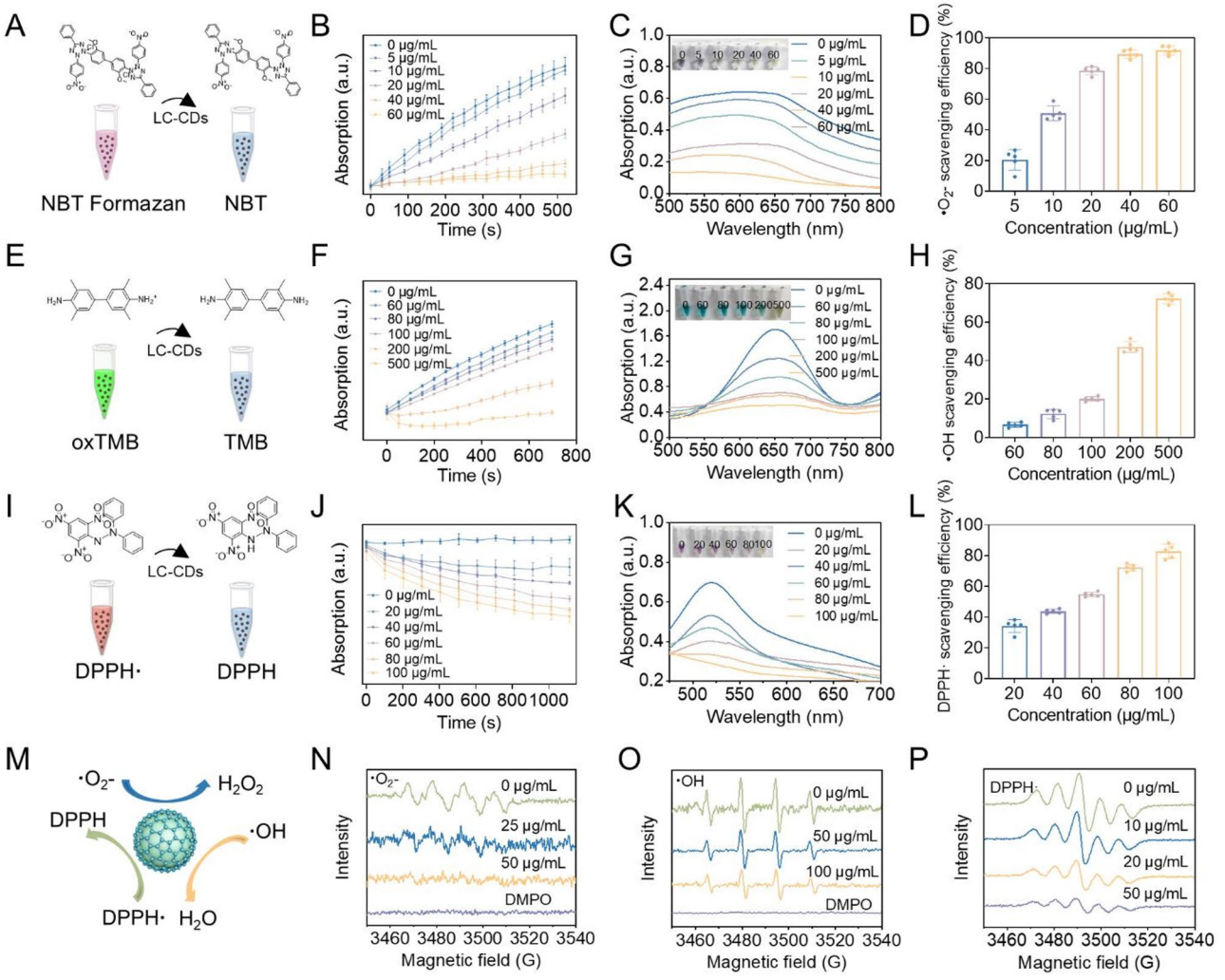

Fig. 4 Free radical scavenging evaluation of LC-CDs. (**A**) Schematic diagram of superoxide radical scavenging system. (**B**) Kinetic curves of $\cdot O_2^-$ scavenged by LC-CDs. (**C**) UV absorption spectra of $\cdot O_2^-$ scavenged by LC-CDs. (**D**) The scavenging rate of $\cdot O_2^-$ by LC-CDs. (**E**) Schematic diagram of ·OH scavenging system. (**F**) Kinetic curves of ·OH scavenged by LC-CDs. (**G**) UV absorption spectra of ·OH scavenged by LC-CDs. (**H**) The scavenging rate of ·OH by LC-CDs. (**I**) Schematic diagram of DPPH· scavenging system. (**J**) Kinetic curves of DPPH· scavenged by LC-CDs. (**K**) UV absorption spectra of DPPH· scavenged by LC-CDs. (**L**) The scavenging rate of DPPH· by LC-CDs. (**M**) Schematic diagram of the scavenging of three types of free radicals by LC-CDs. (**N**-**P**) EPR Spectra Detect the Scavenging of $\cdot O_2^-$, ·OH, and DPPH· by LC-CDs. Data are expressed as mean ± SD ($n = 3$)

generation of ·OH using the Fenton reaction between Fe^{2+} and H_2O_2. In this system, 3,3',5,5'-tetramethylbenzidine (TMB) was used as a chromogenic substance (Fig. 4E). After being oxidized to oxTMB, the solution turns green and can be detected at 652 nm by a microplate reader. Consistent kinetic detection outcomes indicated that with the progressive increase in the concentration of LC-CDs, the oxidation rate of TMB in the solution exhibited a gradual deceleration. This finding corroborated the fact that LC-CDs possess a definite capacity for scavenging·OH (Fig. 4F). Further, we detected the UV absorption spectrum of reaction systems with different LC-CDs concentrations in the range of 500–800 nm. The data revealed that when the concentration of LC-CDs reached 500 μg/mL, TMB was hardly oxidized (Fig. 4G). The statistical results showed that high-concentration LC-CDs can achieve a scavenging rate of nearly 80% for ·OH (Fig. 4H).

Thereafter, we evaluated the scavenging effect of LC-CDs on nitrogen-containing radicals. 1,1-Diphenyl-2-picrylhydrazyl radical (DPPH·) is a typical nitrogen-containing radical. The lone-pair electrons of DPPH· have strong absorption in the visible light region (515–520 nm), making the solution purple (Fig. 4I). The kinetic results showed that the scavenging effect of LC-CDs on DPPH· is concentration-dependent. As time increased, LC-CDs at different concentrations all demonstrated scavenging efficiency for DPPH· (Fig. 4J). The UV absorption spectrum results showed that as the concentration of LC-CDs reached 100 μg/mL, the solution almost faded,

indicating that DPPH· in the solution had been completely scavenged (Fig. 4K). The statistical results also confirmed that as the concentration of LC-CDs reached 100 μg/mL, the scavenging rate for DPPH· could reach approximately 80% (Fig. 4L). Next, we used electron paramagnetic resonance (EPR) technology to further detect the scavenging effect of LC-CDs on $\cdot O_2^-$, ·OH, and DPPH· (Fig. 4N-P). The qualitative results indicated that LC-CDs have a good scavenging effect on these three radicals, and it is concentration-dependent. All the above-mentioned results suggest that LC-CDs possess strong antioxidant capacity (Fig. 4M). Given the typical pathological feature of ROS burst during myocardial ischemia-reperfusion, the antioxidant properties of LC-CDs are expected to show potential application value in the prophylaxis and management strategies for this disease.

Sub-organelle co-localization and antioxidant properties of LC-CDs in cells

Upon myocardial ischemia-reperfusion, the restoration of nutrient and oxygen supply, however, exacerbates the generation of ROS [37]. The instantaneous burst of ROS disrupts the redox homeostasis in the local cardiac region, thereby causing damage to myocardial cells and further inducing inflammatory responses [38]. In this process, the interaction between inflammation and ROS jointly aggravates the MIRI. To thoroughly investigate the repair efficacy of LC-CDs on MIRI, this study systematically examined the antioxidant and anti-inflammatory capacities of LC-CDs at the cellular level. Firstly, the commonly used immune cell model, Raw264.7 cells, was selected to explore the localization of LC-CDs within subcellular organelles. The burst of ROS usually originates from mitochondria. In the mitochondrial respiratory chain, when electrons fail to transfer smoothly to coenzyme Q, they will leak out and directly react with molecular oxygen, generating a large amount of $\cdot O_2^-$, ultimately leading to redox imbalance [39]. Because of this, this study first evaluated the colocalization of LC-CDs with mitochondria. In order to achieve direct visualization of liquid-phase LC-CDs using fluorescence microscopy, this study employed a chemical modification method to attach the fluorescent dye Cy5.5-amino to the surface of LC-CDs. After incubation treatment, the fluorescence emitted by mitochondria and LC-CDs could be clearly observed under a confocal laser scanning microscope. Through the image merging operation, a large number of overlapping regions between them were presented (Fig. 5A). Fluorescence colocalization analysis showed that the Pearson correlation coefficient of colocalization between mitochondria and LC-CDs was as high as 0.98 (Fig. S3A, B). This result fully confirms that LC-CDs are highly localized in mitochondria, and this localization characteristic facilitates their efficient scavenging of ROS. Subsequently, we evaluated the colocalization of LC-CDs with lysosomes. The results indicated that LC-CDs exhibited a certain degree of colocalization with lysosomes, but compared with mitochondria, the colocalization effect was relatively weaker (Fig. 5B). Through analysis, the colocalization coefficient of LC-CDs with lysosomes was 0.79 (Fig. S3C, D). The above results suggest that LC-CDs are more likely to localize in mitochondria and relatively easy to escape from lysosomes. Subsequently, this study employed flow cytometry to evaluate the uptake of LC-CDs by Raw264.7 and H9C2 cells. It was found that after 1-hour incubation, the uptake rate of LC-CDs by Raw264.7 cells could reach 64.10%, and that by H9C2 cells could reach 36.80% (Fig. 5C, D). As the incubation time prolonged, the uptake of LC-CDs by both cell types increased significantly. Next, an OGD/R model was constructed at the cellular level in this study to simulate the oxidative stress induced by ischemia-reperfusion. The 2',7'-dichlorodihydrofluorescein (DCFH) probe was utilized to monitor the intracellular ROS level. When the intracellular oxygen pressure increased, DCFH was oxidized to DCF, which emits strong green fluorescence. The results showed that oxidative stress was successfully induced in H9C2 cells under OGD/R treatment. However, after treatment with LC-CDs, the fluorescence intensity of DCF was significantly weakened (Fig. 5E). Meanwhile, dihydroethidium (DHE) was applied to specifically assess the concentration of $\cdot O_2^-$ in cells, and the results demonstrated that LC-CDs could also significantly scavenge $\cdot O_2^-$ induced by OGD/R (Fig. 5F). The flow cytometry results strongly confirmed that LC-CDs possess remarkable antioxidant ability in the OGD/R model (Fig. 5G, H). Furthermore, this study used H_2O_2 to induce Raw264.7 cells to construct a secondary oxidative stress cell model. Similarly, DCFH and DHE were used to detect the levels of ROS and $\cdot O_2^-$ in Raw264.7 cells. The findings demonstrated that in treatment with LC-CDs, the levels of ROS and $\cdot O_2^-$ in Raw264.7 cells decreased significantly (Fig. 5I, J). The results from flow cytometry further quantified the ability of LC-CDs to scavenge ROS within cells. The flow cytometry results showed that LC-CDs could even reduce the level of $\cdot O_2^-$ to that of the control group (Fig. 5K, L). Similarly, the results obtained from fluorescence statistics of fluorescent images also support the above conclusion (Fig. 5M-P). The above series of results fully confirm that LC-CDs also possess strong antioxidant ability at the cellular level.

Cytoprotective effect of LC-CDs

Multiple studies have demonstrated that macrophages are prone to polarize into M1-type macrophages under the stimulation of ROS. M1-type macrophages secrete a large amount of pro-inflammatory cytokines, which exacerbate the degree of damage following myocardial

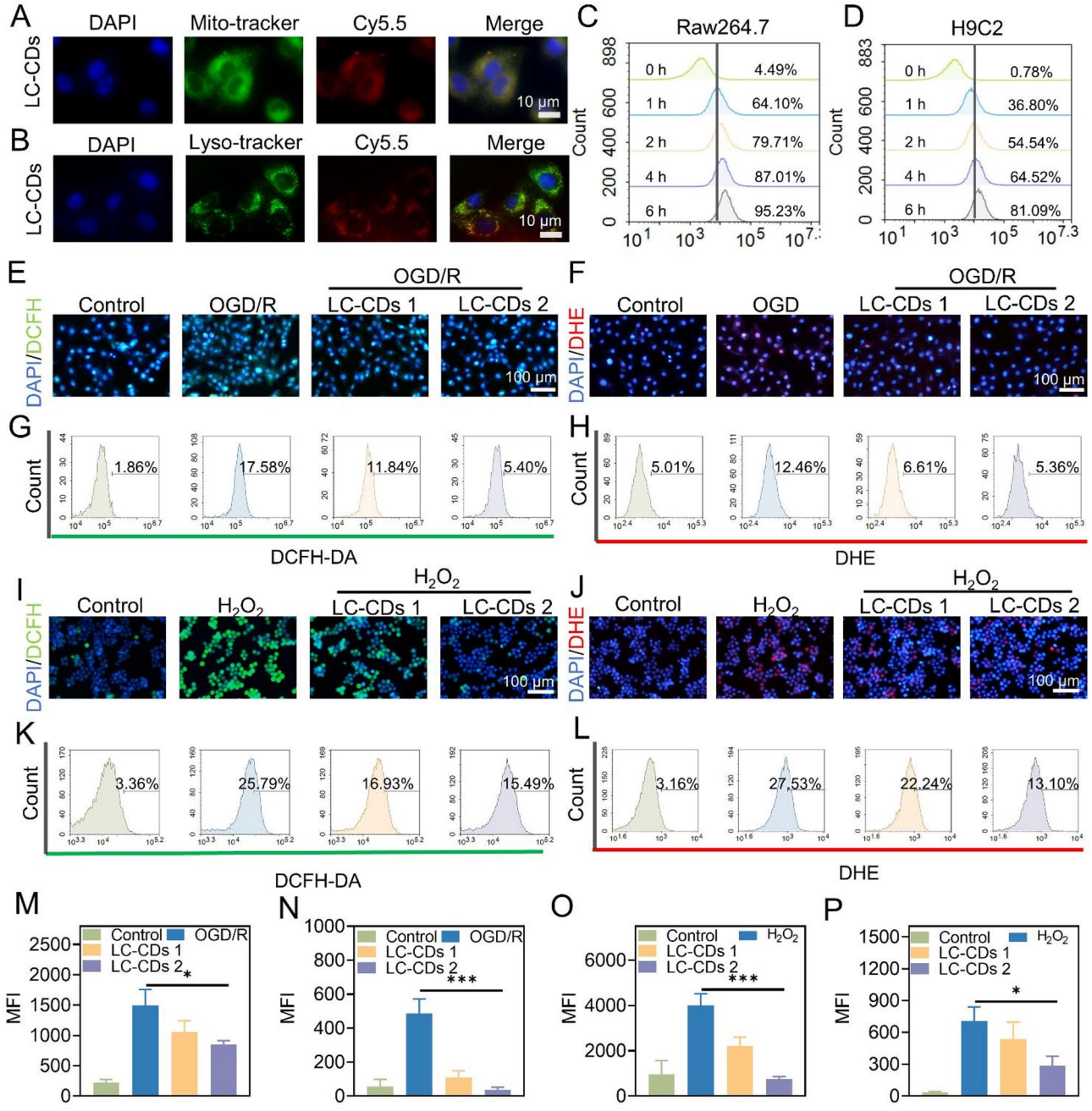

Fig. 5 Sub-organelle co-localization and antioxidant properties of LC-CDs in cells. (**A**) Fluorescence colocalization of LC-CDs with mitochondria. (**B**) Fluorescence colocalization of LC-CDs with lysosomes. (**C** and **D**) Flow cytometric analysis of the uptake of LC-CDs by Raw264.7 cells and H9C2 cells at different times. (**E** and **F**) Fluorescence images of different groups of H9C2 cells incubated with DCFH and DHE. (**G** and **H**) Flow analysis results of different groups of H9C2 cells incubated with DCFH and DHE. (**I** and **J**) Fluorescence images of different groups of Raw264.7 cells incubated with DCFH and DHE. (**K** and **L**) Flow analysis results of different groups of Raw264.7 cells incubated with DCFH and DHE. (**M** and **N**) MFI statistics after incubation of DCFH and DHE with H9C2 cells in different groups. (**O** and **P**) MFI statistics after incubation of DCFH and DHE with Raw264.7 cells in different groups. LC-CDs 1: inducer + 5 μg/mL LCCDs; LC-CDs 2: inducer + 10 μg/mL LC-CDs. Statistical comparisons were made using one-way ANOVA and a t-test. Statistical significance was indicated as $^{*}p < 0.05$, $^{**}p < 0.01$, $^{***}p < 0.001$. Data are expressed as mean ± SD ($n = 3$)

ischemia-reperfusion [40–42]. In this study, lipopolysaccharide (LPS) was employed to induce Raw264.7 cells to construct an M1-type macrophage model, and the cell-surface marker CD86 was selected to identify M1-type macrophages. The results of immunofluorescence detection showed that after treatment with LPS, LC-CDs at different concentrations could significantly inhibit the over-expression of CD86 on the surface of macrophages, and this result was also confirmed by flow cytometry experiments (Fig. 6A, B). Moreover, the large number

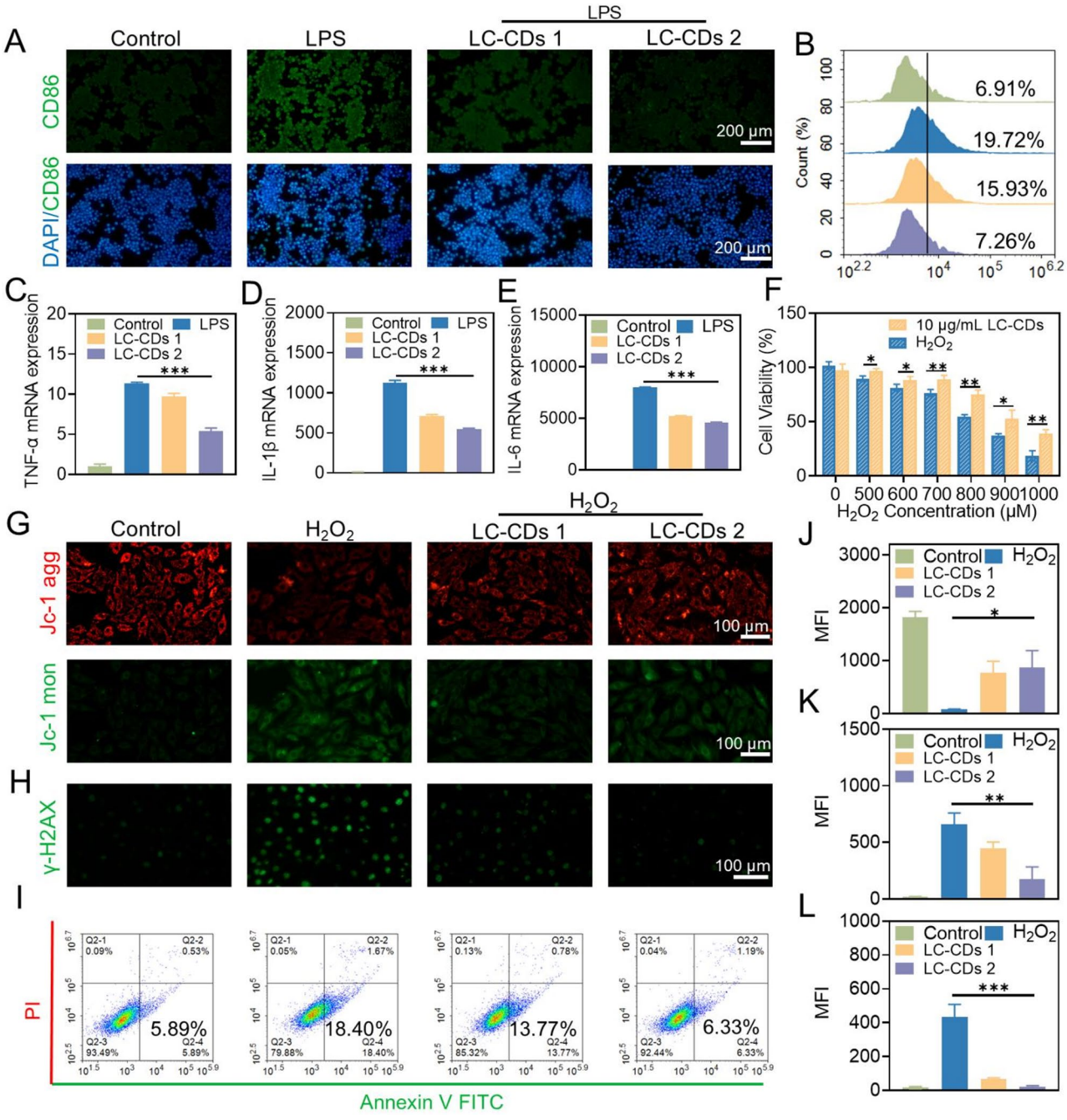

Fig. 6 Evaluation of the cytoprotective effect of LC-CDs. (**A**) Fluorescent images of Raw264.7 cells labeled with CD86 in different treatment groups. (**B**) Flow cytometry results of Raw264.7 cells labeled with CD86 in different treatment groups. (**C**-**E**) qPCR analysis of pro-inflammatory cytokines (TNF-α, IL-1β, and IL-6) in different treatment groups. (**F**) Cell viability of different treatment groups. (**G**) Fluorescent images of JC-1 probe staining in different treatment groups (JC-1 agg: red; JC-1 mon: green). (**H**) Fluorescent images of γ-H2AX labeling in different treatment groups. (**I**) Flow cytometry results of Raw264.7 cells stained with Annexin V FITC/PI in different treatment groups. (**J** and **K**) MFI statistics of JC-1 probe staining in different treatment groups. (**L**) MFI statistics of γ-H2AX labeling in different treatment groups. LC-CDs 1: inducer + 5 μg/mL LC-CDs; LC-CDs 2: inducer + 10 μg/mL LC-CDs. Statistical comparisons were made using one-way ANOVA and a t-test. Statistical significance was indicated as $^{*}p < 0.05$, $^{**}p < 0.01$, $^{***}p < 0.001$. Data are expressed as mean ± SD ($n = 3$)

of inflammatory cytokines secreted by M1-type macrophages aggravates the pathological process of myocardial ischemia-reperfusion. Based on this, this study evaluated the effect of LC-CDs on the release of pro-inflammatory cytokines (such as TNF-α, IL-1β, and IL-6) by Raw264.7 cells at the gene-expression level. The results of real-time fluorescence qPCR indicated that, under the stimulation of LPS, the expression of TNF-α, IL-1β, and IL-6 in

Raw264.7 cells was significantly upregulated; while subsequent treatment with varying concentrations of LC-CDs resulted in a dose-dependent suppression of these inflammatory markers (Fig. 6C-E). This fully demonstrates that LC-CDs can significantly inhibit the occurrence of the immune response of Raw264.7 cells under stimulated conditions. The oxidative damage caused by myocardial ischemia-reperfusion is usually irreversible. Given that the antioxidant and anti-inflammatory effects of LC-CDs have been evaluated previously, it is hypothesized that LC-CDs possess a certain ability to resist oxidative damage. The different concentrations of H_2O_2 were used to induce oxidative stress in cells, thereby triggering cell death. The results of the 3-(4,5-dimethylthiazol-2-yl)-2,5-diphenyltetrazolium bromide (MTT) assay showed that LC-CDs at a concentration of 10 μg/mL could effectively reverse the cell death induced by H_2O_2 (Fig. 6F). During ischemia-reperfusion injury, ROS overproduction targets unsaturated fatty acids within the mitochondrial membrane, causing structural and functional damage that impairs ion and metabolite transport [43]. In this study, the JC-1 fluorescent probe was employed to evaluate changes in mitochondrial membrane potential in H9C2 cells following H_2O_2 stimulation. It was found that after H_2O_2 stimulation, the JC-1 aggregates decreased significantly, and the JC-1 monomers increased, indicating that oxidative stress damaged the mitochondrial membrane and severely disrupted mitochondrial function (Fig. 6G). However, after treatment with LC-CDs at different concentrations, the mitochondrial membrane potential underwent a notable restoration, and the results of fluorescence statistical analysis also supported this conclusion (Fig. 6J, K). During ischemia-reperfusion injury, a reduction in mitochondrial membrane potential triggers cytochrome C translocation into the cytoplasm, leading to the activation of apoptosis-related proteins. LC-CDs protect the energy-metabolism core structure of myocardial cells and effectively prevent the occurrence of apoptosis by maintaining the mitochondrial membrane potential under oxidative stress. After myocardial ischemia-reperfusion, the intense oxidative stress imbalance and inflammatory response can lead to severe DNA damage [44]. In particular, ROS can react with DNA bases and deoxyribose, causing damage to bases, glycosyl groups, and chains, ultimately leading to severe cell apoptosis and myocardial fibrosis. Immunofluorescence staining was used to detect the protective effect of LC-CDs on DNA damage induced by H_2O_2, with γ-H2AX as a marker of DNA damage. The findings revealed that LC-CDs at different concentrations suppressed γ-H2AX expression, suggesting their ability to mitigate oxidative stress-induced DNA damage in cells (Fig. 6H, L). In addition, the Annexin V/propidium iodide (PI) staining method was applied to identify early and late apoptosis of cells. During early apoptosis, cell membrane integrity is compromised, leading to the translocation of phosphatidylserine from the inner to the outer membrane surface. Annexin V can bind to phosphatidylserine (PS) on the outer side of the cell membrane, enabling the identification of early-apoptotic cells by flow cytometry. Flow cytometry analysis revealed that LC-CDs effectively suppressed H_2O_2-induced early apoptosis. As the concentration of LC-CDs attained 10 μg/mL, it could almost completely inhibit the early apoptosis of cells (Fig. 6I). In conclusion, the above-mentioned research results indicate that LC-CDs have a protective effect against mitochondrial damage, DNA damage, and cell apoptosis caused by oxidative stress. These effects are crucial during the process of MIRI, implying that LC-CDs may have a promising application prospect in the therapy for MIRI.

The therapeutic effect of LC-CDs on the MIRI model

Given the remarkable anti-oxidative damage and anti-inflammatory effects of LC-CDs at the cellular level, this investigation set up a rat model of myocardial ischemia-reperfusion to assess the therapeutic efficacy of LC-CDs at the animal level. The model was constructed through surgery (Fig. 7A). Specifically, blood flow in the left anterior descending coronary artery was occluded, followed by restoration after 45 min to simulate the myocardial ischemia-reperfusion process. Meanwhile, in situ administration was performed on the rat heart. Three days after administration, the rats underwent transthoracic echocardiography and were then euthanized. To ensure the stability of the model, the electrocardiogram (ECG) of the rats was continuously monitored during the study. During the myocardial ischemia phase, the membrane potential of the ischemic myocardial cells decreases, creating a potential difference from the normal myocardium. This led to the generation of an injury current, causing the ST-segment elevation in the electrocardiogram leads. Therefore, ST-segment elevation is the most prominent electrocardiogram feature of myocardial ischemia. During the 45-minute myocardial ischemia period, the ST segment of the rat heart electrocardiogram was significantly elevated (Fig. 7B). The instant the blood flow was restored, the ST segment decreased, which fully demonstrated the successful construction of the rat myocardial ischemia-reperfusion model. In the treatment phase, this study selected two concentrations of LC-CDs (1 mg/kg and 5 mg/kg) to treat the rats to evaluate their efficacy. LC-CDs were administered to rats via local myocardial injection. When myocardial injury occurs, the cell membrane permeability increases, and creatine kinase (CK) and lactate dehydrogenase (LDH) are released into the blood. The levels of CK and LDH in the blood are crucial indicators for evaluating cardiac function. Based on this, the study collected the serum of treated rats at the

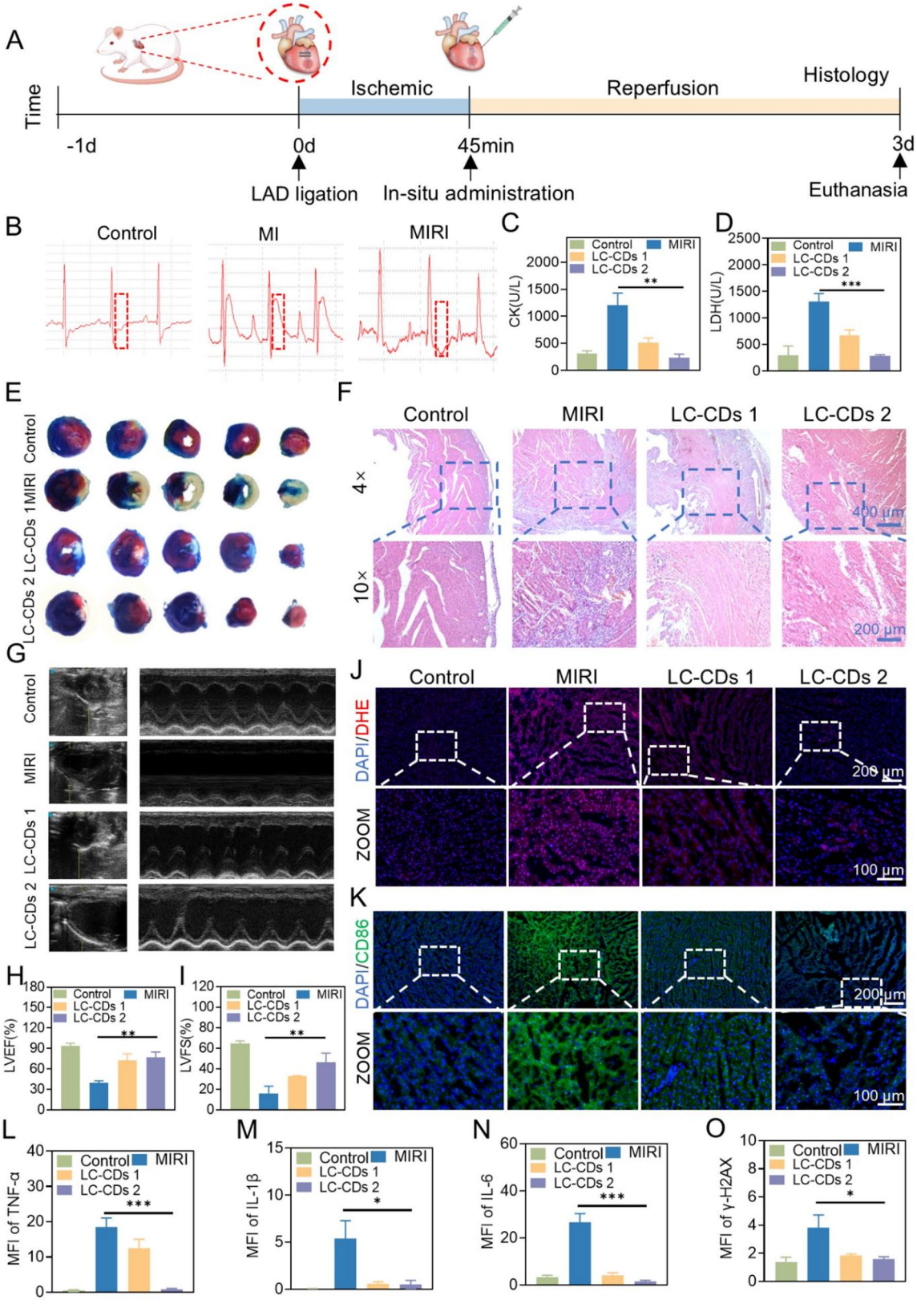

Fig. 7 (See legend on next page.)

(See figure on previous page.)

Fig. 7 The therapeutic effect of LC-CDs on MIRI. (**A**) Schematic diagram of the experimental procedure. (**B**) Electrocardiogram during the establishment of rat MIRI mode. (**C** and **D**) Contents of CK and LDH in the blood of rats in different treatment groups. (**E**) Evans blue/TTC staining of heart sections from rats in different treatment groups. (**F**) H&E pathological section staining of the hearts of rats in different treatment groups. (**G**) Transthoracic echocardiography of rats in different treatment groups. (**H** and **I**) LVEF and LVFS of the hearts of rats in different treatment groups. (**J** and **K**) DHE and CD86 immunofluorescence staining of the hearts of rats in different treatment groups. (**L**-**O**) Statistics of fluorescence intensity of immunofluorescence staining (TNF-α, IL-1β, IL-6, and γ-H2AX). LC-CDs 1: MIRI + 1 mg/kg LC-CDs; LC-CDs 2: MIRI + 5 mg/kg LC-CDs. Statistical comparisons were made using one-way ANOVA and t-test. Statistical significance was indicated as $^{*}p < 0.05$, $^{**}p < 0.01$, $^{***}p < 0.001$. Data are expressed as mean ± SD ($n = 3$)

identical time point for blood biochemical analysis. The results showed that myocardial injury led to a marked elevation in the levels of CK and LDH in the blood of the MIRI group rats. After treatment with different concentrations of LC-CDs, these two indicators significantly decreased, indicating that the cardiac function of the treated rats was improved (Fig. 7C, D). To analyze the infarct area of the rat heart after treatment, this study employed the TTC (2,3,5-triphenyltetrazolium chloride) and Evans blue staining methods. TTC can be reduced to red triphenylformazan (TPF) by dehydrogenases in living tissues, while dead cells cannot reduce TTC and thus appear white. Evans blue can stain the normally perfused areas of the rat heart tissue blue, and the non-stained areas are the at-risk areas of blood supply. In the at-risk areas, the parts stained white by TTC are the infarct areas. The staining results of different sections of the rat heart in the MIRI group showed that the rat heart had severe infarction, and almost all of the at-risk areas were infarcted (Fig. 7E). After treatment with LC-CDs, the infarct area in the at-risk areas decreased. After treatment with a high concentration of LC-CDs, the infarct area in the at-risk areas almost returned to normal (Fig. 7E). Given the outstanding therapeutic efficacy of LC-CDs, this study employed paraffin-embedded tissue sectioning and hematoxylin-eosin (H&E) staining to assess inflammatory cell infiltration in rat cardiac tissue. The results showed that in the infarct area of the MIRI group, a large number of inflammatory cell infiltrations and tissue damage were visible (Fig. 7F). This damage to the myocardial microenvironment was irreversible. After treatment with different concentrations of LC-CDs, the inflammatory infiltration in the infarct area was significantly reduced. Meanwhile, LC-CDs also reduced the blood cell leakage caused by ischemia-reperfusion. To evaluate the impact of LC-CDs on the physiological function of the rat heart, before euthanizing the rats, transthoracic echocardiography was used to measure the cardiac function parameters of rats in different groups, including left ventricular ejection fraction (LVEF), left ventricular fractional shortening (LVFS) (Fig. 7G). As depicted in Fig. 7H, in comparison with the healthy group (LVEF: 93.45% ± 4.29), the echocardiogram of the MIRI group rats showed weakened left ventricular anterior wall motion (LVEF: 39.99% ± 2.5%), indicating that the myocardial injury caused by myocardial ischemia-reperfusion might lead to cardiac systolic dysfunction. Fortunately, after in situ injection of LC-CDs, the left ventricular anterior wall motion of the rat heart was significantly restored. The LVFS of the low-concentration treatment group reached 72.22% ± 10%, and that of the high-concentration treatment group was 76.62% ± 8.41%. At the same time, the LVFS of the MIRI group significantly decreased (16.01% ± 7.15%). After treatment with LC-CDs, the LVFS also significantly recovered, and the high-concentration treatment group could reach 46.62% ± 8.60% (Fig. 7I). These results fully demonstrated that LC-CDs could repair the myocardial injury caused by myocardial ischemia and thus restore cardiac function. The oxidative stress state in the local area of the heart was further verified by the DHE probe. After ischemia-reperfusion, a vast amount of ROS bursts occurred at the damaged site of the heart. After treatment with LC-CDs, the ROS level was significantly reduced, greatly alleviating the oxidative damage to myocardial cells (Fig. 7J). Oxidative damage is often accompanied by immune infiltration. The previous H&E staining results have proven that LC-CDs can inhibit immune cell infiltration. Further, by labeling the surface marker CD86 of M1-type macrophages, the changes in M1-type macrophages in the infarct area of the heart were observed. The data indicated a notable rise in CD86 expression in the MIRI group, whereas LC-CDs treatment led to its reduction, suggesting a decline in M1-type macrophage levels within the cardiac tissue following LC-CDs administration (Fig. 7K). The flow cytometry results of M1 and M2 labeling of myocardial cells in different treatment groups show that after treatment with LC-CDs, it can not only reduce the M1 polarization of macrophages but also promote the M2 polarization of macrophages (Fig. S4). In addition, immunofluorescence was used to detect the expression levels of pro-inflammatory cytokines (TNF-α, IL-1β, and IL-6) in the heart tissue after different treatments. The findings revealed elevated expression levels of these three pro-inflammatory cytokines in the MIRI group, with varying degrees of upregulation. In contrast, the LC-CDs treatment group markedly decreased the levels of these pro-inflammatory cytokines, contributing to the stabilization of the cardiac immune microenvironment (Fig. S5B-D). The fluorescence statistical data also supported this conclusion (Fig. 7L-N). The qPCR results of the myocardial tissues also demonstrated the anti-inflammatory effectiveness of LC-CDs (Fig. S6). Meanwhile, immunofluorescence of γ-H2AX was also used to detect the DNA damage of myocardial cells (Fig.

S5A). As expected, in the myocardial infarct area, the myocardial cells in the MIRI group had extensive DNA damage, while LC-CDs significantly inhibited this damage (Fig. 7O). In conclusion, LC-CDs markedly alleviate cardiac dysfunction induced by myocardial ischemia and shield myocardial cells against oxidative stress-induced injury. At the same time, it can inhibit immune cell infiltration, lower the synthesis of pro-inflammatory cytokines, and ultimately achieve rapid repair after myocardial ischemia-reperfusion.

RNA sequencing to explore biological mechanisms of LC-CDs

To deeply explore the specific mechanisms underlying the treatment of MIRI by LC-CDs, this study conducted RNA sequencing (RNA-seq) analysis on the treated rat hearts. The results of principal component analysis (PCA) clearly presented the differences among the three treatment groups: the Control group, the MIRI group, and the LC-CDs treatment group. Among them, the MIRI group exhibited the most pronounced differences in gene expression compared to the other two groups, whereas the heart tissue treated with LC-CDs displayed a profile closer to the control group (Fig. 8A). The gene-expression heatmap further revealed that there were significant gene-expression differences among the three treatment groups (Fig. 8B). Although there were also certain gene-expression differences among the three samples within each group, considering that this difference might be attributed to the natural inter-individual variations, it had no substantial impact on the final results. Subsequently, the gene-expression profiles of rat hearts treated with LC-CDs were compared with those of the MIRI group. The volcano plot revealed a substantial number of genes with differential expression across the two sample groups (Fig. 8C). After treatment with LC-CDs, a total of 1058 genes were upregulated, and 894 genes were downregulated. The results of gene ontology (GO) and Kyoto Encyclopedia of Genes and Genomes (KEGG) enrichment analyses for these differentially expressed genes are presented as follows. In the GO analysis, biological processes were the key focus. The results revealed that differentially expressed genes were notably associated with biological processes including immune and inflammatory responses, blood pressure regulation, blood vessel development, and superoxide anion production (Fig. 8D). This suggests that LC-CDs primarily modulate disease progression during MIRI repair by targeting pathways involved in immune regulation and superoxide radical production. In the KEGG enrichment analysis, the specific signaling pathways affected by LC-CDs were identified, including ECM-receptor interaction, IL-17 signaling pathway, NOD-like receptor signaling pathway, MAPK signaling pathway, NF-kappa B signaling pathway, TNF signaling pathway, JAK-STAT signaling pathway, and HIF-1 signaling pathway (Fig. 8E). Next, to further verify the effect of LC-CDs on the aforementioned signaling pathways, we carried out a more in-depth statistical analysis of the key downstream genes within these signaling pathways. The results showed that after treatment with LC-CDs, the expression levels of the key genes in these pathways all returned to the same state as those of the control group. This result strongly indicates that LC-CDs can effectively regulate the relevant signaling pathways (Fig. S7). In addition, gene-set enrichment analysis (GSEA) provided a comprehensive assessment of differential gene expression at the gene-set level. The GSEA results showed that two pathways, oxidative phosphorylation and Negative regulation of the apoptosis process, underwent significant changes after LC-CDs treatment (Fig. 8F, G). This discovery aligns with the outcomes of previous network-pharmacology analyses regarding the mechanisms by which Ligusticum Chuanxiong affects MIRI. Furthermore, western blotting results demonstrated that LC-CDs inhibited apoptosis through down-regulation of key proteins, including Caspase3, Caspase9, and Bax (Fig. 8H).

Biosafety evaluation of LC-CDs

The biosafety of ultrasmall carbon nanoparticles has always been a focus in the research field. This study first investigated the effects of LC-CDs on Raw264.7 cells and H9C2 cells at the cellular level. Encouragingly, even when the concentration of LC-CDs reached 200 μg/mL, the MTT assay results showed that after 24-hour co-incubation with Raw264.7 cells, the cell viability remained greater than 80% (Fig. 9A). Similarly, in the H9C2 cell experiment, H9C2 cells also maintained good cell viability after co-incubation with LC-CDs (Fig. 9B). Regarding blood safety, it was evaluated through a hemolysis experiment. After co-incubating different concentrations of LC-CDs with blood cells for 4 h, no abnormal phenomena were observed in the blood cells, indicating that LC-CDs had good safety in the blood (Fig. 9C). To assess the in vivo safety of LC-CDs in animals, LC-CDs were injected in situ into the rat hearts. After three consecutive days of observation, the drug-administered group exhibited a normal growth trend in body weight compared to the healthy group (Fig. 9D). Pathological sections of the main organs of rats, including the heart, liver, spleen, lungs, and kidneys, were prepared and observed by H&E staining. The findings indicated that the heart tissue and other major organs in the drug-administered group exhibited no significant pathological alterations, confirming that LC-CDs did not induce severe damage to these organs (Fig. 9E, F). Furthermore, the effects of LC-CDs on the functions of the main organs were evaluated through blood biochemical and blood routine tests.

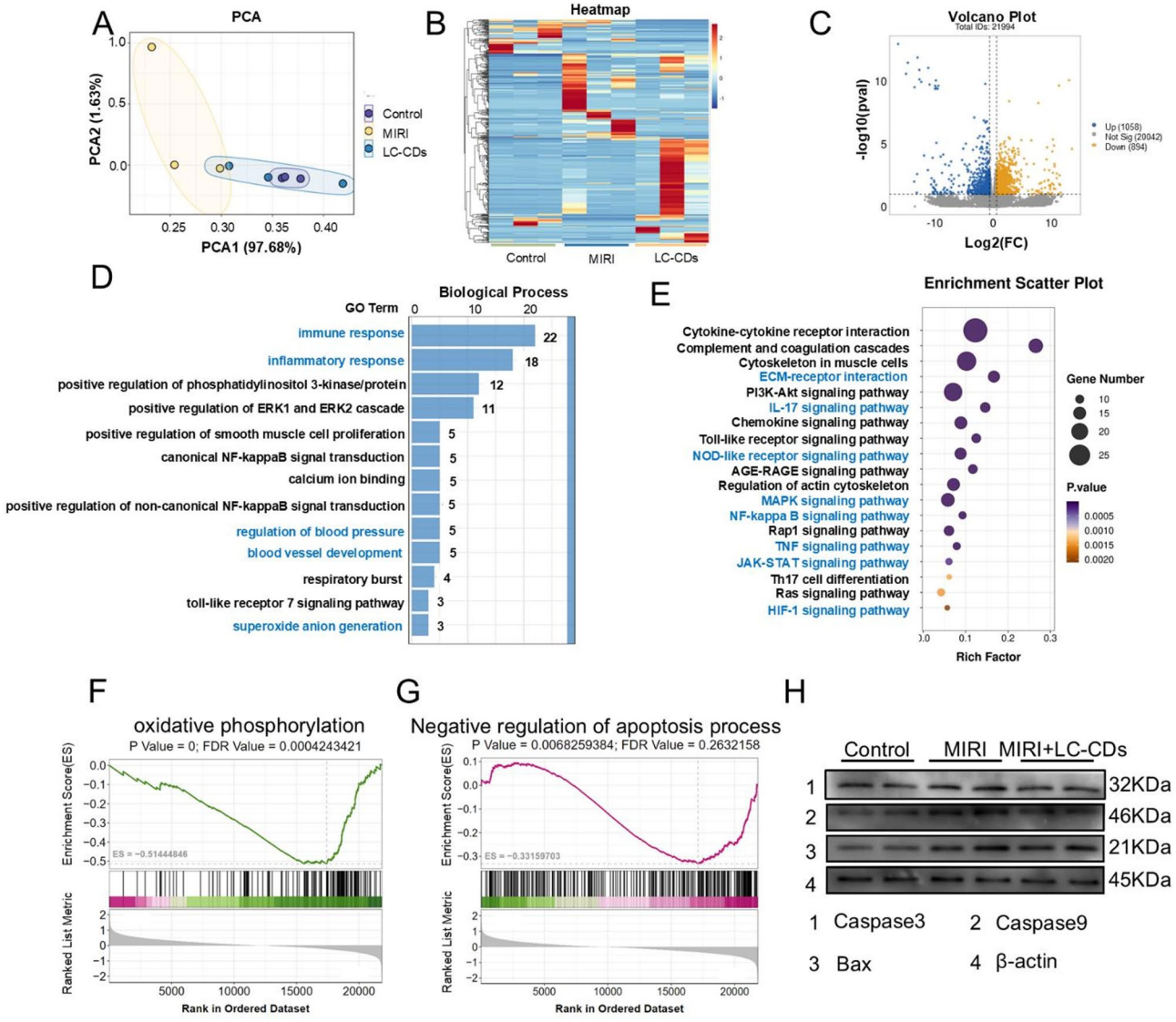

Fig. 8 RNA sequencing to explore biological mechanisms of LC-CDs. (**A**) PCA analysis of the Control, MIRI, and MIRI + LC-CDs groups. (**B**) Heat map of genes in different treatments. (**C**) Volcano plots of all genes in the MIRI + LC-CDs group and the MIRI group. The blue dots represented the upregulated differently expressed genes, the yellow dots were downregulated differently expressed genes, and the grey dots were non-differentially expressed genes. (**D**) GO enrichment of differential genes in MIRI + LC-CDs and MIRI groups. (**E**) KEGG enrichment of differential genes in MIRI + LC-CDs and MIRI groups. (**F** and **G**) GSEA enrichment analysis of differentially expressed genes (oxidative phosphorylation and Negative regulation of apoptosis process). (**H**) Expression of key proteins in the apoptosis pathway (Caspase3, Caspase9, and Bax)

Analysis of blood biochemical indicators showed no significant differences in levels of Total Protein, Alanine Aminotransferase, and other markers between the drug-administered group and the control or healthy groups, suggesting that LC-CDs did not significantly affect liver function (Fig. 9G). The Albumin and Globulin indicators also showed no differences, suggesting that LC-CDs did not trigger an immune response in rats. The normal Glucose and Urea indicators indicated that the blood-glucose level and kidney function of the drug-administered group of rats were not impaired (Fig. 9G). The blood-routine indicators showed that there were no obvious differences in the blood conditions between the LC-CDs-treated group of rats and the healthy rats (Fig. 9H). In summary, the above results fully demonstrate that LC-CDs possess excellent biosafety.

Conclusion

In the present investigation, LC-CDs were successfully fabricated via a one-step hydrothermal approach, utilizing the Chinese herbal medicine Ligusticum Chuanxiong as a carbon-material precursor. A thorough assessment of their therapeutic potential for MIRI was subsequently conducted. LC-CDs, owing to their robust

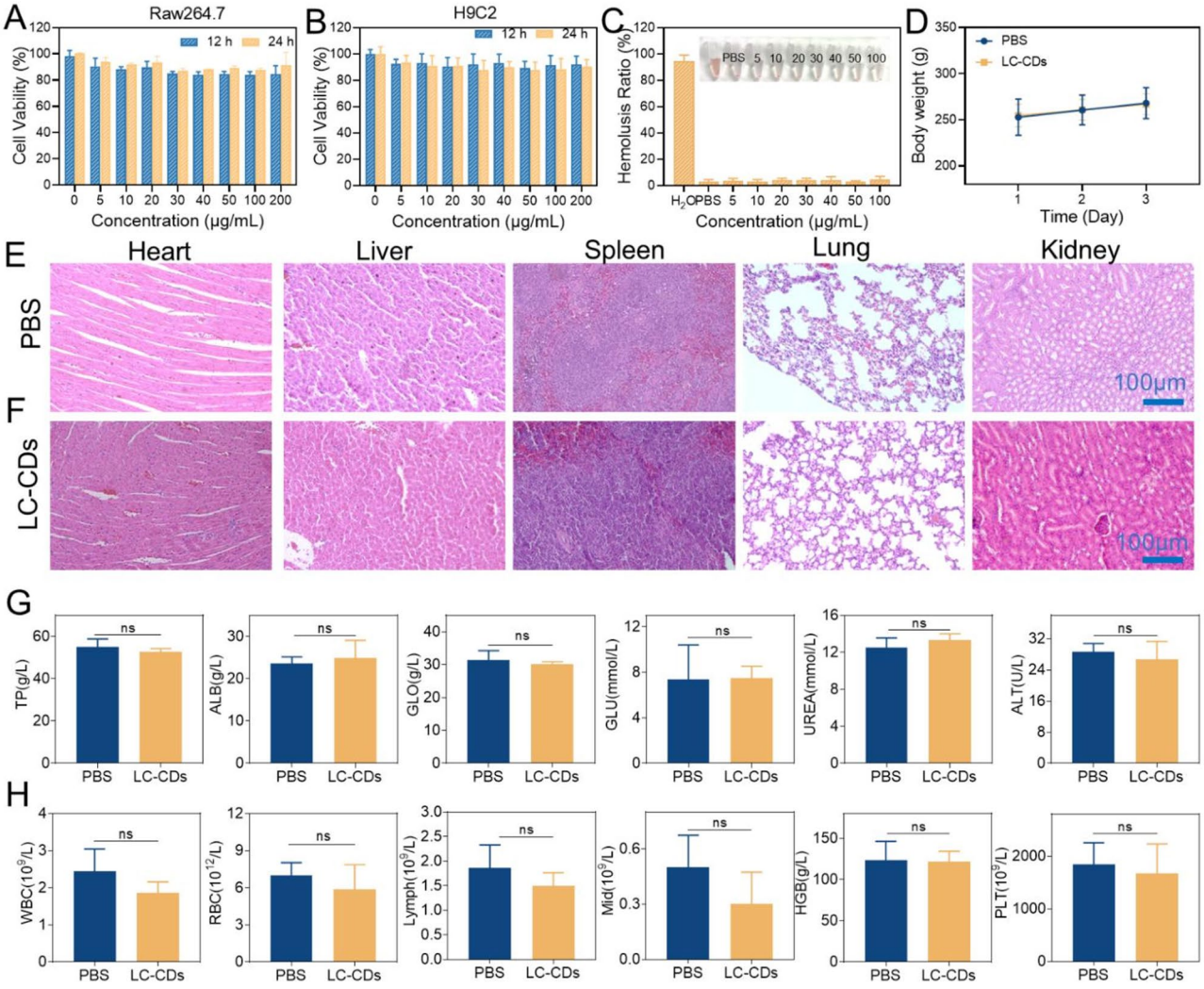

Fig. 9 Biosafety evaluation of LC-CDs. (**A**) Cell viability of different concentrations of LC-CDs incubated with Raw264.7 for 12 h and 24 h. (**B**) Cell viability of different concentrations of LC-CDs incubated with H9C2 for 12 h and 24 h. (**C**) Hemolysis test. (**D**)Changes in body weight of rats in different treatment groups ($n=3$ mice). (**E**) H&E staining of major organs for biosafety in healthy groups of mice. (**F**) H&E staining of major organs for biosafety in the LC-CDs groups of mice. (**G**) Blood biochemistry analysis results of the above mice. (**H**) Complete blood panel analysis results of LC-CDs-treated mice. Statistical comparisons were made using one-way ANOVA and t-test. "ns" represents "no statistically significant difference". Data are expressed as mean ± SD ($n=3$)

ROS scavenging capacity, efficiently alleviate the oxidative stress burden within cells and significantly curtail oxidative cellular damage. Systematic analyses employing network pharmacology and transcriptomics revealed congruent mechanisms of action between LC-CDs and Ligusticum Chuanxiong. Both entities were found to mitigate MIRI by suppressing the cellular apoptotic pathway. Specifically, LC-CDs demonstrated remarkable efficacy in attenuating MIRI, promoting cardiac function recovery by alleviating oxidative stress and inhibiting apoptosis. The synthesis of LC-CDs represents an innovative solution, effectively circumventing the challenges associated with the clinical application of Ligusticum Chuanxiong, including its suboptimal bioavailability and the arduous process of active ingredient extraction. Moreover, given that Ligusticum chuanxiong has a clinical application history spanning thousands of years, the raw materials of LC-CDs possess superior biosecurity when compared to those of other carbon-based or metal-based nanomaterials. This study innovatively combines the unique advantages of traditional Chinese medicine with modern nanotechnology, and LC-CDs are obtained through a simple and efficient synthesis method. This novel material is anticipated to offer a valuable example for clinical MIRI treatment strategies and pave the way for further advancements in this field.

Supplementary Information

The online version contains supplementary material available at https://doi.org/10.1186/s12951-025-03477-w.

Supplementary Material 1

Acknowledgements
We thank Dr. Zijun Ren at the Instrument Analysis Center of Xi'an Jiaotong University for assisting with TEM analysis and Dr. Xiaofei Wang at the experimental biomedical center of Xi'an Jiaotong University for his kind assistance with the instrument operation and data analysis. The authors would like to acknowledge the critical and quantity of testing work supported by Beijing Zhongkebaice Technology Service Co., Ltd. (www.zkbaice.cn). We thank Laboratory Animal Center of Xi'an jiaotong University for their assistance with Laboratory animal.

Author contributions
Yapeng Guo: Investigation, Methodology, Writing-original draft. Lei Yang: Methodology, Data curation. Li Yao: Conceptualization, Methodology, Formal analysis. Chengdong Zhou: Conceptualization, Methodology, Formal analysis. Yuanyuan Zhu: Investigation, Data curation. Chenxi Xu: Data curation. Wenlong Wang: Writing-review & editing. Jian Song: Methodology. Zhichao Deng: Writing review & editing, Resources, Supervision. Mingzhen Zhang: Conceptualization, Writing-review & editing, Resources, Supervision, Funding acquisition, Project administration.

Funding
This work was supported by the National Natural Science Foundation of China (Nos. 82472127, 32360176), Shaanxi Health Research Fund Project (2022D019), the "Young Talent Support Plan" of Xi'an Jiaotong University, China (No YX6J001), Natural Science Foundation of Shaanxi Province (2024JC-YBMS-781), and the Bagui Scholars Program of Guangxi Zhuang Autonomous Region.

Data availability
No datasets were generated or analysed during the current study.

Declarations

Ethics approval and consent to participate
All animal experiments followed the Principles of Laboratory Animal Care and Guidelines of the Laboratory Animal Care Committee of Xi'an Jiaotong University (No: 2024 – 151).

Consent for publication
Not applicable.

Competing interests
The authors declare no competing interests.

Received: 2 April 2025 / Accepted: 19 May 2025
Published online: 29 May 2025

References

1. Reed GW, Rossi JE, Cannon CP. Acute myocardial infarction. Lancet. 2017;389:197–210.
2. Hausenloy DJ, Erik Bøtker H, Condorelli G, Ferdinandy P, Garcia-Dorado D, Heusch G, Lecour S, van Laake LW, Madonna R, Ruiz-Meana M, et al. Translating cardioprotection for patient benefit: position paper from the working group of cellular biology of the heart of the European society of cardiology. Cardiovasc Res. 2013;98:7–27.
3. Arzamendi D, Benito B, Tizon-Marcos H, Flores J, Tanguay JF, Ly H, Doucet S, Leduc L, Leung TK, Campuzano O, et al. Increase in sudden death from coronary artery disease in young adults. Am Heart J. 2011;161:574–80.
4. Anderson JL, Morrow DA. Acute myocardial infarction. N Engl J Med. 2017;376:2053–64.
5. Alistar A, Morris BB, Desnoyer R, Klepin HD, Hosseinzadeh K, Clark C, Cameron A, Leyendecker J, D'Agostino R Jr., Topaloglu U, et al. Safety and tolerability of the first-in-class agent CPI-613 in combination with modified FOLFIRINOX in patients with metastatic pancreatic cancer: a single-centre, open-label, dose-escalation, phase 1 trial. Lancet Oncol. 2017;18:770–8.
6. De Bock K, Georgiadou M, Carmeliet P. Role of endothelial cell metabolism in vessel sprouting. Cell Metab. 2013;18:634–47.
7. Savchenko AS, Borissoff JI, Martinod K, De Meyer SF, Gallant M, Erpenbeck L, Brill A, Wang Y, Wagner DD. VWF-mediated leukocyte recruitment with chromatin decondensation by PAD4 increases myocardial ischemia/reperfusion injury in mice. Blood. 2014;123:141–8.
8. Xing N, Long X-T, Zhang H-J, Fu L-D, Huang J-Y, Chaurembo AI, Chanda F, Xu Y-J, Shu C, Lin K-X et al. Research progress on effects of traditional Chinese medicine on myocardial ischemia–reperfusion injury: A review. Front Pharmacol. 2022; 13.
9. Wang G, Dai G, Song J, Zhu M, Liu Y, Hou X, Ke Z, Zhou Y, Qiu H, Wang F et al. Lactone component from Ligusticum Chuanxiong alleviates myocardial ischemia injury through inhibiting autophagy. Front Pharmacol. 2018; 9.
10. Wang R, Wang M, Zhou J, Wu D, Ye J, Sun G, Sun X. Saponins in Chinese herbal medicine exerts protection in myocardial Ischemia–Reperfusion injury: possible mechanism and target analysis. Front Pharmacol. 2021; 11.
11. Huang W, Yang Y, Zeng Z, Su M, Gao Q, Zhu B. Effect of Salvia miltiorrhiza and ligustrazine injection on myocardial ischemia/reperfusion and hypoxia/reoxygenation injury. Mol Med Rep. 2016;14:4537–44.
12. Lin J, Wang Q, Zhou S, Xu S, Yao K. Tetramethylpyrazine: A review on its mechanisms and functions. Biomed Pharmacother. 2022;150:113005.
13. Huang Y, Wu Y, Yin H, Du L, Chen C. Senkyunolide I: A review of its phytochemistry, pharmacology, pharmacokinetics, and Drug-Likeness. Molecules. 2023;28:3636.
14. Chen S-Y, Hsiao G, Hwang H-R, Cheng P-Y, Lee Y-M. Tetramethylpyrazine induces Heme oxygenase-1 expression and attenuates myocardial ischemia/reperfusion injury in rats. J Biomed Sci. 2006;13:731–40.
15. Yang Q, Huang DD, Li DG, Chen B, Zhang LM, Yuan CL, Huang HH. Tetramethylpyrazine exerts a protective effect against injury from acute myocardial ischemia by regulating the PI3K/Akt/GSK-3β signaling pathway. Cell Mol Biol Lett. 2019;24:17.
16. Li J, Liu H, Yang Z, Yu Q, Zhao L, Wang Y. Synergistic effects of Cryptotanshinone and Senkyunolide I in Guanxinning tablet against endogenous Thrombus formation in zebrafish. Front Pharmacol. 2021; 11.
17. Hu Y-y, Wang Y, Liang S, Yu X-l, Zhang L, Feng L-y, Feng Y. Senkyunolide I attenuates oxygen-glucose deprivation/reoxygenation-induced inflammation in microglial cells. Brain Res. 2016;1649:123–31.
18. Nie R, Zhang J, Jia Q, Li Y, Tao W, Qin G, Liu X, Tao Y, Zhang Y, Li P. Structurally oriented carbon Dots as ROS nanomodulators for dynamic chronic inflammation and infection elimination. ACS Nano. 2024;18:22055–70.
19. Wang C, Li J, Liu K, Li J, Zhang F, Ma X, Li Y, Zhang C, Liu X, Qu Y et al. Donkey-Hide Gelatin-Derived carbon Dots activate erythropoiesis and eliminate oxidative stress for aplastic Anemia treatment. ACS Nano. 2025.
20. Yan X, Zhao Y, Luo J, Xiong W, Liu X, Cheng J, Wang Y, Zhang M, Qu H. Hemostatic bioactivity of novel pollen Typhae Carbonisata-derived carbon quantum Dots. J Nanobiotechnol. 2017;15:60.
21. Liang P, Bi T, Zhou Y, Wang C, Ma Y, Xu H, Shen H, Ren W, Yang S. Carbonized Platycladus orientalis derived carbon Dots accelerate hemostasis through activation of platelets and coagulation pathways. Small. 2023;19:2303498.
22. Jiang Y, Zhao T, Xu W, Peng Z. Red/NIR C-dots: A perspective from carbon precursors, photoluminescence tuning and bioapplications. Carbon. 2024;219:118838.
23. Tian B, Liu S, Yu C, Liu S, Dong S, Feng L, Hu N, Yang P. A Metal-Free mesoporous carbon dots/silica hybrid type I photosensitizer with Enzyme-Activity for synergistic treatment of hypoxic tumor. Adv Funct Mater. 2023;33:2300818.
24. Dong J, Liu G, Petrov YV, Feng Y, Jia D, Baulin VE, Yu Tsivadze A, Zhou Y, Li B. Discovery of FeP/Carbon Dots nanozymes for enhanced Peroxidase-Like catalytic and antibacterial activity. Adv Healthc Mater. 2024;13:2402568.
25. Zhang Y, Gao W, Ma Y, Cheng L, Zhang L, Liu Q, Chen J, Zhao Y, Tu K, Zhang M, et al. Integrating Pt nanoparticles with carbon nanodots to achieve robust cascade superoxide dismutase-catalase nanozyme for antioxidant therapy. Nano Today. 2023;49:101768.
26. Liu C, Fan W, Cheng W-X, Gu Y, Chen Y, Zhou W, Yu X-F, Chen M, Zhu M, Fan K, et al. Red emissive carbon Dot superoxide dismutase nanozyme for bioimaging and ameliorating acute lung injury. Adv Funct Mater. 2023;33:2213856.
27. Gao W, He J, Chen L, Meng X, Ma Y, Cheng L, Tu K, Gao X, Liu C, Zhang M, et al. Deciphering the catalytic mechanism of superoxide dismutase activity of carbon Dot nanozyme. Nat Commun. 2023;14:160.
28. Wang H, Mu Q, Wang K, Revia RA, Yen C, Gu X, Tian B, Liu J, Zhang M. Nitrogen and Boron Dual-Doped graphene quantum Dots for Near-Infrared second window imaging and photothermal therapy. Appl Mater Today. 2019;14:108–17.
29. Xia C, Zhong J, Han X, Zhu S, Li Y, Liu H, Yang B. The formation mechanism of carbonized polymer Dots: Crosslinking-Induced nucleation and carbonization. Angew Chem Int Ed Engl. 2024;63:e202410519.

30. Li J, Wang H, Li Y, Wang C, Feng H, Pang Y, Ren J, Li C, Gao E, Zhang D, et al. Novel carbon Dots with dual modulatory effects on the bone marrow and spleen as a potential therapeutic candidate for treating spinal cord injury. Bioact Mater. 2025;45:534–50.
31. Jiang Y, Xiao L, Wang J, Tian T, Liu G, Zhao Y, Guo J, Zhang W, Wang J, Chen C, et al. Carbon nanodots constructed by ginsenosides and their high inhibitory effect on neuroblastoma. J Nanobiotechnol. 2023;21:244.
32. Deng Z, Zhang Y, Li R, Zhu Y, Xu C, Gao B, Wang W, Ding C, He B, Zhu X et al. Honeysuckle-Derived carbon Dots with robust catalytic and Pharmacological activities for mitigating lung inflammation by Inhibition of Caspase11/GSDMD-Dependent pyroptosis. Adv Funct Mater. 2025; 2418683.
33. Yellon DM, Hausenloy DJ. Myocardial reperfusion injury. N Engl J Med. 2007;357:1121–35.
34. Lim CH, Ryan MD, McCarthy BG, Theriot JC, Sartor SM, Damrauer NH, Musgrave CB, Miyake GM. Intramolecular charge transfer and ion pairing in N,N-Diaryl dihydrophenazine photoredox catalysts for efficient organocatalyzed atom transfer radical polymerization. J Am Chem Soc. 2017;139:348–55.
35. Novoselov KS, Geim AK, Morozov SV, Jiang D, Zhang Y, Dubonos SV, Grigorieva IV, Firsov AA. Electric field effect in atomically thin carbon films. Science. 2004;306:666–9.
36. Zhang Y, Tang TT, Girit C, Hao Z, Martin MC, Zettl A, Crommie MF, Shen YR, Wang F. Direct observation of a widely tunable bandgap in bilayer graphene. Nature. 2009;459:820–3.
37. Becker LB. New concepts in reactive oxygen species and cardiovascular reperfusion physiology. Cardiovasc Res. 2004;61:461–70.
38. Coggins M, Rosenzweig A. The fire within: cardiac inflammatory signaling in health and disease. Circ Res. 2012;110:116–25.
39. Alamri S, Siddiqui MH, Kushwaha BK, Singh VP, Ali HM. Mitigation of arsenate toxicity by indole-3-acetic acid in Brinjal roots: plausible association with endogenous hydrogen peroxide. J Hazard Mater. 2021;405:124336.
40. Liu S, Chen J, Shi J, Zhou W, Wang L, Fang W, Zhong Y, Chen X, Chen Y, Sabri A, et al. M1-like macrophage-derived exosomes suppress angiogenesis and exacerbate cardiac dysfunction in a myocardial infarction microenvironment. Basic Res Cardiol. 2020;115:22.
41. Zhang M, Nakamura K, Kageyama S, Lawal AO, Gong KW, Bhetraratana M, Fujii T, Sulaiman D, Hirao H, Bolisetty S et al. Myeloid HO-1 modulates macrophage polarization and protects against ischemia-reperfusion injury. JCI Insight. 2018; 3.
42. Sindrilaru A, Scharffetter-Kochanek K. Disclosure of the culprits: Macrophages-Versatile regulators of wound healing. Adv Wound Care (New Rochelle). 2013;2:357–68.
43. Chu Q, Zhang Y, Zhong S, Gao F, Chen Y, Wang B, Zhang Z, Cai W, Li W, Zheng F et al. N-n-Butyl Haloperidol Iodide Ameliorates Oxidative Stress in Mitochondria Induced by Hypoxia/Reoxygenation through the Mitochondrial c-Jun N-Terminal Kinase/Sab/Src/Reactive Oxygen Species Pathway in H9c2 Cells. Oxid Med Cell Longev. 2019; 2019: 7417561.
44. Wu L, Sowers JR, Zhang Y, Ren J. Targeting DNA damage response in cardiovascular diseases: from pathophysiology to therapeutic implications. Cardiovasc Res. 2023;119:691–709.

Publisher's note